osteoblasts. Osteoclast-lineage cells have also been shown to change the expression levels of chemokines and chemokine receptors after stimulation by RANKL. These chemokines and their receptors probably regulate the migration of the precursors not only onto the bone surface but also to other precursors for fusion in an autocrine/paracrine manner. RANKL induces the expression of C-C chemokines such as CCL2 (or monocyte chemoattractant protein-1, MCP-1) (8;11;13), CCL3 (or macrophage inflammatory protein-1α, MIP-1α) (9;11;26), CCL5 (or regulated on activation, normal T cell expressed and secreted, RANTES) (8;11), and CCL9 (or MIP-1γ) (10;26), as well as C-X-C chemokines such as CXCL2 (or MIP-2α) (11) and CXCL10 (or interferon-γ-inducible 10-kDa protein, IP-10) (11;12). In addition, the chemokine receptors CCR1 (7;8;10;26), CCR2 (7;8;13), CCR3 (10), and CXCR1 (26) are reported to be induced by RANKL. During osteoclastogenesis, some chemokines (for example, CCL3, CCL4, CCL5, CXCL2, and CXCL10) and receptors (such as CCR2 and CX3CR1) are downregulated (5-7;11;12). Presumably, after the cells mature and arrive at their destinations, these chemoattractants have served their function and are no longer needed. Table 1 summarizes the chemokines and their receptors, which are reported to be involved in the migration of osteoclast precursors.

In addition to protein chemokines, we have clarified that sphingosine-1-phosphate (S1P), a lipid mediator enriched in blood, regulates the migration of osteoclast precursors. S1P is synthesized in most cells, but is irreversibly degraded by intracellular S1P lyase or dephosphorylated by S1P phosphatase. Therefore, the levels of S1P in most tissues, including bone marrow, are relatively low. On the other hand, its concentration in the blood is extremely high. In addition, S1P is an amphiphilic molecule that cannot be expelled easily across membranes. In this way, a S1P gradient between the blood and tissues is stably maintained. S1P transmits signals through GPCRs, as do chemokines. Mammals possess five types of S1P receptors, $S1P_1$ to $S1P_5$, and macrophage-monocyte lineage cells express $S1P_1$ and $S1P_2$ (27-29). $S1P_1$ is coupled primarily to PTx-sensitive $G_{i/o}$ proteins, and $S1P_2$ is coupled to $G_{12/13}$, and G_s. These differences account for the different biological effects of $S1P_1$ and $S1P_2$, which have opposite effects on osteoclast precursor migration. Expression levels of $S1P_1$ are reduced by RANKL stimulation, dependent on NF-κB, not NF-AT. Osteoclast precursors show chemoattracting responses to a S1P gradient *in vitro*, which is blocked by PTx. In addition, S1P treatment of osteoclast precursors induced an increase in the active form of Rac (GTP-Rac), suggesting that Rac and Gαi are involved in the $S1P_1$ chemotactic signaling pathway. Additionally, $S1P_1$ agonists promote the recirculation of osteoclast precursors and ameliorate ovariectomy-induced bone loss (14). On the other hand, $S1P_2$ has a binding affinity for S1P that differs from that of $S1P_1$. A higher concentration of S1P is required to activate $S1P_2$, which induced negative chemotactic responses to a S1P gradient and causes the cells to move out of the bloodstream into the bone marrow cavity (unpublished observation).

Seeing Is Believing

Typically, chemotaxis has been assayed using several *in vitro* systems, including transmigration assays using Transwell filters or a Boyden chamber (30). These methods are convenient for determining quantity and are highly reproducible. However, these *in vitro* assay systems may not accurately reflect *in vivo* cellular behavior.

Recent technological progress in fluorescence microscopy, especially two-photon excitation-based laser microscopy, has enabled the visualization of dynamic cell behavior deep inside intact living organs (23;24). With two-photon microscopy, we have observed osteoclast migration by visualizing murine bone marrow in real-time in a living body (14). There are limitations to visualizing the deep tissue of bone, because the crystallized calcium phosphate in the bone matrix scatters both visible and infrared light. However, we have developed

IBMS BoneKEy. 2010 August;7(8):279-286
http://www.bonekey-ibms.org/cgi/content/full/ibmske;7/8/279
doi: 10.1138/20100459

Table 1. Chemoattractants and repellents for osteoclast precursors. The lines indicate possible interactions between the ligands and the receptors. OC: osteoclast; BM: bone marrow.

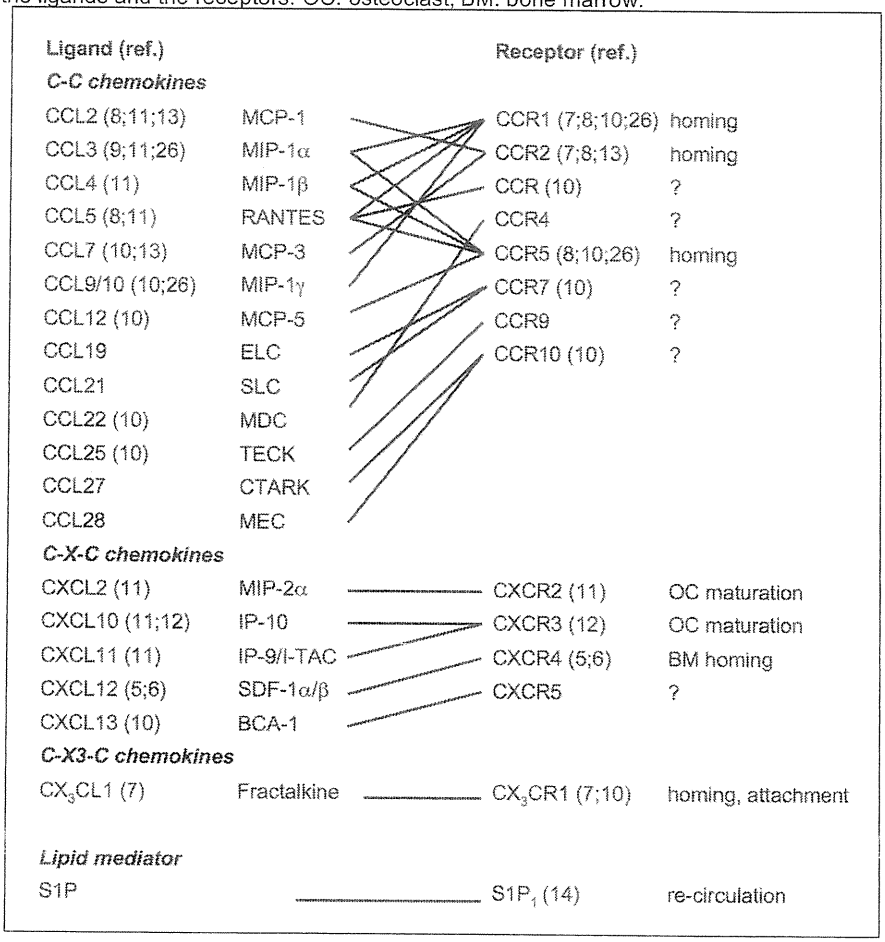

a novel intravital imaging system for visualizing the living bone marrow cavity with high spatiotemporal resolution. We chose the skull of a mouse as the observation site because it is about 100 μm thick, which is within the range of two-photon microscopy (31). Monocytes present in the bone marrow cavity, including osteoclast precursors, are generally stationary. However, a subset of these cells becomes motile shortly after the intravenous application of SEW2871, a selective S1P1 agonist, with some of the mobilized cells entering the blood circulation. Thus, S1P1 agonists promote the recirculation of osteoclast precursor monocytes from the bone surface into the blood, thereby repressing osteoclastogenesis (14;15).

Intravital imaging is making a great contribution to visualizing these animated processes *in vivo*. It provides spatiotemporal information in a living body, which cannot be procured by other methods. This approach has revealed active features of both physiological bone homeostasis and pathological bone destruction. Nevertheless, intravital microscopy imaging has several limitations. First, two-photon microscopy has a penetration depth of up to 200 μm in hard tissues, and thus deeper tissues cannot be observed. Given this resolution limitation, the technique is applicable only in small animal models such as mice and rats, and not in humans. Second, owing to the wide scattering of light on the skin, it is necessary to exteriorize the target organ, and it is difficult to observe tubular bones. To

IBMS BoneKEy. 2010 August;7(8):279-286
http://www.bonekey-ibms.org/cgi/content/full/ibmske;7/8/279
doi: 10.1138/20100459

overcome these limitations, technical innovations in fluorescent probes and optical systems are needed, including improved emission light and resolution.

In the future, in addition to its use in viewing morphology and motion, intravital imaging will be applied to functional analyses. This will be possible by using new photoresponsive fluorescent proteins that change fluorescence upon absorbing light energy of specific wavelengths, *e.g.*, photoactivation (acquiring fluorescence) and photoconversion (changing the wavelength of the emitted light) (32;33), and light-sensing devices such as photo-activating GPCRs (34;35).

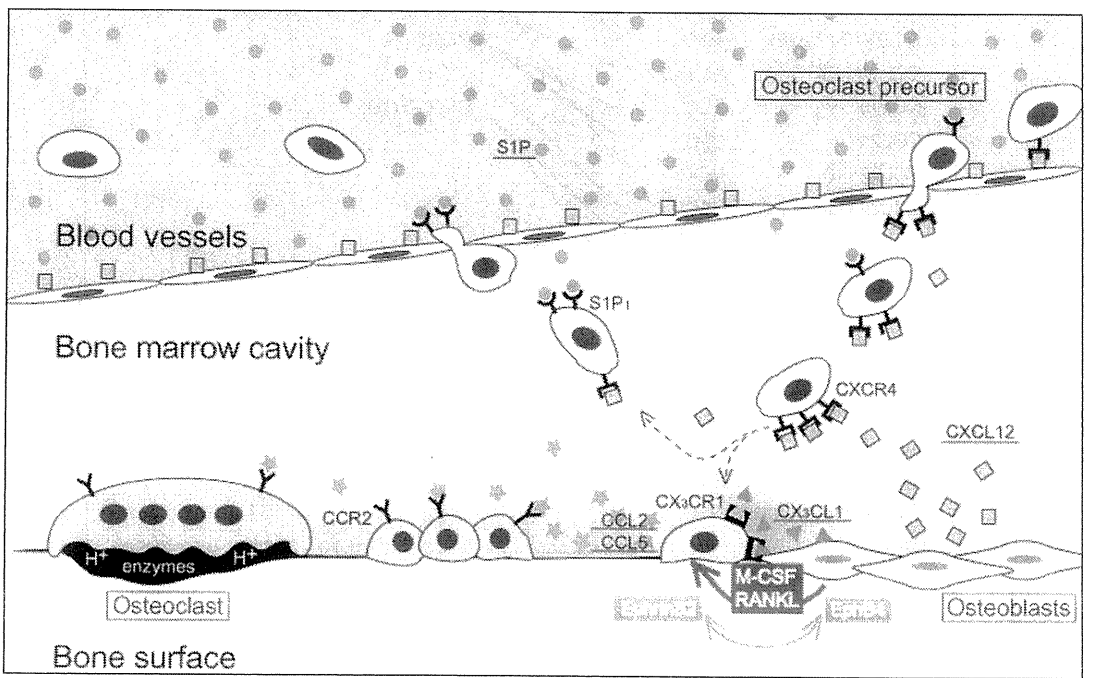

Fig. 1. Several chemoattractants control the behavior of monocyte/macrophage-lineage osteoclast precursors. Bone-attraction molecules such as CXCL12 attract osteoclast precursors into the bone marrow cavity from the bloodstream. Then, bone-attachment inducers such as CX3CL1 recruit and attach the precursors to the bone surface, where they resorb bone. Finally, paracrine effectors such as CCL2 and CCL5 cause the precursor cells to fuse with each other. Circular-attraction molecules such as S1P drive the cells out of the bone marrow cavity and into the bloodstream. To maintain bone homeostasis, these processes regulate the number of osteoblastic stromal cell-derived osteoclast precursors on the bone surface that are available for stimulation by M-CSF, RANKL, or Eph.

Conclusion

Osteoclastogenesis can be considered to occur in three steps: 1) recruitment of precursors; 2) cell fusion; and 3) bone resorption. Of these, cell recruitment is the most dynamic step and the most dependent on the microenvironment of the bone marrow cavity. The results achieved so far are summarized in Fig. 1. Briefly, the regulation of monocyte-lineage osteoclast precursor migration is critical for the development of osteoclasts and the maintenance of bone homeostasis. Several chemokines recruit osteoclast precursors to sites of resorption, and cause them to fuse with each other, and other circular-attraction molecules such as S1P drive osteoclast precursors out of the bone marrow cavity. Given the importance of temporospatial information in elucidating these processes, intravital imaging has made a huge contribution. For example, this new technique has revealed that several

chemoattractants act in concert to shepherd osteoclast precursors to appropriate sites. Controlling the recruitment and migration of osteoclast precursors can be a promising new therapeutic target for bone diseases. In addition, intravital imaging will afford new opportunities for studying both the physiology and pathology of bone.

Conflict of Interest: None reported.

Peer Review: This article has been peer-reviewed.

References

1. Harada S, Rodan GA. Control of osteoblast function and regulation of bone mass. *Nature*. 2003 May 15;423(6937):349-55.

2. Teitelbaum SL, Ross FP. Genetic regulation of osteoclast development and function. *Nat Rev Genet*. 2003 Aug;4(8):638-49.

3. Wada T, Nakashima T, Hiroshi N, Penninger JM. RANKL-RANK signaling in osteoclastogenesis and bone disease. *Trends Mol Med*. 2006 Jan;12(1):17-25.

4. Henriksen K, Neutzsky-Wulff AV, Bonewald LF, Karsdal MA. Local communication on and within bone controls bone remodeling. *Bone*. 2009 Jun;44(6):1026-33.

5. Yu X, Huang Y, Collin-Osdoby P, Osdoby P. Stromal cell-derived factor-1 (SDF-1) recruits osteoclast precursors by inducing chemotaxis, matrix metalloproteinase-9 (MMP-9) activity, and collagen transmigration. *J Bone Miner Res*. 2003 Aug;18(8):1404-18.

6. Wright LM, Maloney W, Yu X, Kindle L, Collin-Osdoby P, Osdoby P. Stromal cell-derived factor-1 binding to its chemokine receptor CXCR4 on precursor cells promotes the chemotactic recruitment, development and survival of human osteoclasts. *Bone*. 2005 May;36(5):840-53.

7. Koizumi K, Saitoh Y, Minami T, Takeno N, Tsuneyama K, Miyahara T, Nakayama T, Sakurai H, Takano Y, Nishimura M, Imai T, Yoshie O, Saiki I. Role of CX3CL1/fractalkine in osteoclast differentiation and bone resorption. *J Immunol*. 2009 Dec 15;183(12):7825-31.

8. Kim MS, Day CJ, Morrison NA. MCP-1 is induced by receptor activator of nuclear factor-kappaB ligand, promotes human osteoclast fusion, and rescues granulocyte macrophage colony-stimulating factor suppression of osteoclast formation. *J Biol Chem*. 2005 Apr 22;280(16):16163-9.

9. Choi SJ, Cruz JC, Craig F, Chung H, Devlin RD, Roodman GD, Alsina M. Macrophage inflammatory protein 1-alpha is a potential osteoclast stimulatory factor in multiple myeloma. *Blood*. 2000 Jul 15;96(2):671-5.

10. Lean JM, Murphy C, Fuller K, Chambers TJ. CCL9/MIP-1gamma and its receptor CCR1 are the major chemokine ligand/receptor species expressed by osteoclasts. *J Cell Biochem*. 2002;87(4):386-93.

11. Ha J, Choi HS, Lee Y, Kwon HJ, Song YW, Kim HH. CXC chemokine ligand 2 induced by receptor activator of NF-kappaB ligand enhances osteoclastogenesis. *J Immunol*. 2010 May 1;184(9):4717-24.

12. Kwak HB, Ha H, Kim HN, Lee JH, Kim HS, Lee S, Kim HM, Kim JY, Kim HH, Song YW, Lee ZH. Reciprocal cross-talk between RANKL and interferon-gamma-inducible protein 10 is responsible for bone-erosive experimental arthritis. *Arthritis Rheum*. 2008 May;58(5):1332-42.

13. Binder NB, Niederreiter B, Hoffmann O, Stange R, Pap T, Stulnig TM, Mach M, Erben RG, Smolen JS, Redlich K. Estrogen-dependent and C-C chemokine receptor-2-dependent pathways determine osteoclast behavior

in osteoporosis. *Nat Med.* 2009 Apr;15(4):417-24.

14. Ishii M, Egen JG, Klauschen F, Meier-Schellersheim M, Saeki Y, Vacher J, Proia RL, Germain RN. Sphingosine-1-phosphate mobilizes osteoclast precursors and regulates bone homeostasis. *Nature*. 2009 Mar 26;458(7237):524-8.

15. Germain RN, Bajénoff M, Castellino F, Chieppa M, Egen JG, Huang AY, Ishii M, Koo LY, Qi H. Making friends in out-of-the-way places: how cells of the immune system get together and how they conduct their business as revealed by intravital imaging. *Immunol Rev*. 2008 Feb;221:163-81.

16. Lacey DL, Timms E, Tan HL, Kelley MJ, Dunstan CR, Burgess T, Elliott R, Colombero A, Elliott G, Scully S, Hsu H, Sullivan J, Hawkins N, Davy E, Capparelli C, Eli A, Qian YX, Kaufman S, Sarosi I, Shalhoub V, Senaldi G, Guo J, Delaney J, Boyle WJ. Osteoprotegerin ligand is a cytokine that regulates osteoclast differentiation and activation. *Cell*. 1998 Apr 17;93(2):165-76.

17. Yasuda H, Shima N, Nakagawa N, Yamaguchi K, Kinosaki M, Mochizuki S, Tomoyasu A, Yano K, Goto M, Murakami A, Tsuda E, Morinaga T, Higashio K, Udagawa N, Takahashi N, Suda T. Osteoclast differentiation factor is a ligand for osteo-protegerin/osteoclastogenesis-inhibitory factor and is identical to TRANCE/RANKL. *Proc Natl Acad Sci U S A*. 1998 Mar 31;95(7):3597-602.

18. Kong YY, Yoshida H, Sarosi I, Tan HL, Timms E, Capparelli C, Morony S, Oliveira-dos-Santos AJ, Van G, Itie A, Khoo W, Wakeham A, Dunstan CR, Lacey DL, Mak TW, Boyle WJ, Penninger JM. OPGL is a key regulator of osteoclastogenesis, lymphocyte development and lymph-node organogenesis. *Nature*. 1999 Jan 28;397(6717):315-23.

19. Zhao C, Irie N, Takada Y, Shimoda K, Miyamoto T, Nishiwaki T, Suda T, Matsuo K. Bidirectional ephrinB2-EphB4 signaling controls bone homeostasis. *Cell Metab*. 2006 Aug;4(2):111-21.

20. McClung MR, Lewiecki EM, Cohen SB, Bolognese MA, Woodson GC, Moffett AH, Peacock M, Miller PD, Lederman SN, Chesnut CH, Lain D, Kivitz AJ, Holloway DL, Zhang C, Peterson MC, Bekker PJ; AMG 162 Bone Loss Study Group. Denosumab in postmenopausal women with low bone mineral density. *N Engl J Med*. 2006 Feb 23;354(8):821-31.

21. Cummings SR, San Martin J, McClung MR, Siris ES, Eastell R, Reid IR, Delmas P, Zoog HB, Austin M, Wang A, Kutilek S, Adami S, Zanchetta J, Libanati C, Siddhanti S, Christiansen C; FREEDOM Trial. Denosumab for prevention of fractures in postmenopausal women with osteoporosis. *N Engl J Med*. 2009 Aug 20;361(8):756-65.

22. Mizoguchi T, Muto A, Udagawa N, Arai A, Yamashita T, Hosoya A, Ninomiya T, Nakamura H, Yamamoto Y, Kinugawa S, Nakamura M, Nakamichi Y, Kobayashi Y, Nagasawa S, Oda K, Tanaka H, Tagaya M, Penninger JM, Ito M, Takahashi N. Identification of cell cycle-arrested quiescent osteoclast precursors in vivo. *J Cell Biol*. 2009 Feb 23;184(4):541-54.

23. Cahalan MD, Parker I, Wei SH, Miller MJ. Two-photon tissue imaging: seeing the immune system in a fresh light. *Nat Rev Immunol*. 2002 Nov;2(11):872-80.

24. Germain RN, Miller MJ, Dustin ML, Nussenzweig MC. Dynamic imaging of the immune system: progress, pitfalls and promise. *Nat Rev Immunol*. 2006 Jul;6(7):497-507.

25. Rot A, von Andrian UH. Chemokines in innate and adaptive host defense: basic chemokinese grammar for immune

cells. *Annu Rev Immunol*. 2004;22:891-928.

26. Ishida N, Hayashi K, Hattori A, Yogo K, Kimura T, Takeya T. CCR1 acts downstream of NFAT2 in osteoclastogenesis and enhances cell migration. *J Bone Miner Res*. 2006 Jan;21(1):48-57.

27. Rosen H, Goetzl EJ. Sphingosine 1-phosphate and its receptors: an autocrine and paracrine network. *Nat Rev Immunol*. 2005 Jul;5(7):560-70.

28. Rivera J, Proia RL, Olivera A. The alliance of sphingosine-1-phosphate and its receptors in immunity. *Nat Rev Immunol*. 2008 Oct;8(10):753-63.

29. Cyster JG. Chemokines, sphingosine-1-phosphate, and cell migration in secondary lymphoid organs. *Annu Rev Immunol*. 2005;23:127-59.

30. Boyden S. The chemotactic effect of mixtures of antibody and antigen on polymorphonuclear leucocytes. *J Exp Med*. 1962 Mar 1;115:453-66.

31. Cavanagh LL, Bonasio R, Mazo IB, Halin C, Cheng G, van der Velden AW, Cariappa A, Chase C, Russell P, Starnbach MN, Koni PA, Pillai S, Weninger W, von Andrian UH. Activation of bone marrow-resident memory T cells by circulating, antigen-bearing dendritic cells. *Nat Immunol*. 2005 Oct;6(10):1029-37.

32. Lippincott-Schwartz J, Patterson GH. Development and use of fluorescent protein markers in living cells. *Science*. 2003 Apr 4;300(5616):87-91.

33. Remington SJ. Fluorescent proteins: maturation, photochemistry and photophysics. *Curr Opin Struct Biol*. 2006 Dec;16(6):714-21.

34. Wu YI, Frey D, Lungu OI, Jaehrig A, Schlichting I, Kuhlman B, Hahn KM. A genetically encoded photoactivatable Rac controls the motility of living cells. *Nature*. 2009 Sep 3;461(7260):104-8.

35. Airan RD, Thompson KR, Fenno LE, Bernstein H, Deisseroth K. Temporally precise in vivo control of intracellular signalling. *Nature*. 2009 Apr 23;458(7241):1025-9.

Intravital two-photon imaging: a versatile tool for dissecting the immune system

Taeko Ishii, Masaru Ishii

Laboratory of Biological Imaging, WPI-Immunology Frontier Research Center, Osaka University, Osaka, Japan

Correspondence to
Dr Masaru Ishii, Laboratory of Biological Imaging, WPI-Immunology Frontier Research Center, Osaka University, 3-1 Yamada-oka, Suita, Osaka 565-0871, Japan;
mishii@ifrec.osaka-u.ac.jp

Accepted 8 August 2010

ABSTRACT

During the past decade, multi-photon or 'two-photon' excitation microscopy has launched a new era in the field of biological imaging. The near-infrared excitation laser for two-photon microscopy can penetrate thicker specimens, enabling the visualisation of living cell behaviour deep within tissues and organs without thin sectioning. The minimised photobleaching and toxicity enables the visualisation of live and intact specimens for extended periods. In this brief review, recent findings in intravital two-photon imaging for the physiology and pathology of the immune system are discussed. The immune system configures highly dynamic networks, where many cell types actively travel throughout the body and interact with each other in specific areas. Hence, real-time intravital imaging may be a powerful tool for dissecting the mechanisms of this dynamic system.

The most unique characteristic of the immune system is its highly dynamic nature. A variety of cell types, such as lymphocytes, macrophages and dendritic cells (DCs), are continuously circulating throughout the body, migrating through the peripheral tissues and interacting with each other in their respective niches. Conventional methodologies in immunology, such as flow cytometry, cell or tissue culture, biochemistry and histology, have brought tremendous achievement within this field, although the dynamics of immune cells in an entire animal remain less clear.

Technological progress of fluorescence microscopy has enabled us to visualise the intact biological phenomenon that has been uninvestigated. Among the advancements, the recent emergence and prevalence of two-photon, excitation-based, laser microscopy has revolutionised the research field, such that the dynamic behaviour of cells deep inside living organs can be visualised and analysed.

ADVANTAGES OF TWO-PHOTON IMAGING

Here we briefly describe the advantages of the two-photon microscopy compared with conventional (single-photon) confocal microscopy.[1–4] In confocal microscopy, upon excitation, a fluorophore molecule absorbs energy from a single photon and thereafter releases the energy as an emission photon. In contrast, in two-photon excitation, a fluorophore absorbs two photons simultaneously. Such an event rarely occurs, and can only occur in areas of high photon density. Based on this principle, two-photon microscopy can spatially confine the excitation area to the focal point of an objective lens, which concentrates photons into a very small area. The spatiotemporally restricted excitation provides many advantages over confocal microscopy for biological imaging. First, bright and high-resolution images can be obtained of regions deep inside tissues and organs. Because near-infrared lasers for two-photon excitation can penetrate deeper with less absorption or scattering than visible or UV light as used with confocal microscopy, objects can be visualised at a depth of 100–1000 μm with two-photon microscopy, whereas areas <100 μm are accessed with confocal microscopy. This capacity is especially useful for dissecting live tissues and organs. A broader range of tissue can be seen using conventional microscopy if the specimen is fixed and thin-sectioned, but the cells in the section are dead and not moving. To visualise the cells moving in live specimens, the areas to be analysed are sometimes lying deep inside. In such cases, two-photon excitation microscopy enables one to see the inside from the surface without fixation or thin-sectioning. In addition, excitation with near-infrared lasers can minimise photobleaching, the destruction of fluorophores and phototoxicity-induced tissue damage, which is beneficial for live imaging over an extended period of time.

Another advantage of two-photon microscopy is the non-linear optical effects such as second-harmonic generation.[4 5] Owing to the intensity of the laser passing through a highly polarised material, second-harmonic emission at precisely half the wavelength of the original light is generated. Using near-infrared lasers for two-photon excitation, the second-harmonic emission is in the range of the visible wavelength. Because many intrinsic biological structures, including collagen fibre, muscle, brain, cornea and bone, induce this kind of effect, these structures can be visualised without labelling them with exogenous probes.

Two-photon excited in vivo real-time imaging has revolutionised biology. In the following sections, we summarise findings in the field of immunology, focusing on the physiology and pathology of the immune system.

IMAGING OF THE IMMUNE SYSTEM

Lymphoid tissues

One of the first applications of two-photon imaging of the immune system was an explanted lymph node.[6] It was reported that naive T cells showed higher mobility than B cells in an intact lymph node, and that their speed was as rapid as 25 μm/min. These results challenged the previous belief that T cells were immobile without antigen stimulation. Further observations have modified the 'random-walk model' of T cells to a model of 'organised migration', probably because unstained objects such as other cells, stroma and the reticular network could not be detected.[3 7 8]

Real-time observations have also shown that T cells change their migration behaviour upon contact with antigen-presenting cells.[7 8] At the induction of priming, when T cells encounter activated antigen-presenting DCs during their rapid movement in a lymph node, they make stable complexes that last for several hours at least. Subsequently, the T cells become motile again. On the other hand, during tolerance induction, T cells have much shorter sustained contact with DCs.

Conventionally, it has been assumed that B-cell proliferation occurs only in the germinal centre and that activated T cells, with decreased expression of C–C chemokine receptor 7 (CCR7) and increased expression of C–X–C chemokine receptor 5 (CXCR5), migrate towards B-cell follicles to help promote antibody production. Interestingly, real-time imaging has shown that B cells upregulate CCR7 expression and migrate to the boundary of the follicle.[7 9]

Intravital imaging has disclosed these dynamic interactions, but two important questions remain: What contributes to the differences between priming and tolerance? What regulates the differences in interaction times?

Thymus

In thymic organ cultures, two-photon microscopy has shown interactions between thymocyte and stromal cells during positive and negative selection.[10] The immature CD4 CD8 double-positive thymocytes localise in the outer cortex. During positive selection, they become $CD4CD8^-$ or $CD4^-CD^8$ single-positive thymocytes, and migrate to the central medulla. Real-time imaging revealed that thymocytes were highly motile and that major histocompatibility complex (MHC) recognition by thymocytes was associated with both stable and dynamic contacts with thymic stromal cells. The different interaction patterns could be associated with different signals or could correspond to different stages of positive selection. After positive selection, the thymocyte population displayed rapid, directed migration toward the medulla.[10] Compared with thymocytes in the cortex, the medullary thymocytes migrated limitlessly and more rapidly, and made frequent and transient contacts with DCs. During negative selection, thymocytes migrated slowly and in a highly confined manner within zones of up to 30 μm in diameter.[11]

Bone marrow

There is an inherent limitation to visualising the deep tissue of bone, because both visible and infrared light are easily scattered by crystallised calcium phosphate in the bone matrix.[12–14] However, the mouse skull is only 100 μm thick, which is thin enough to be within the range of two-photon microscopy. A pilot study showed that central memory CD8 T cells were preferentially recruited to, and accumulated in, the bone marrow cavity and interacted with mature circulating DCs.[13 14]

We have developed a novel intravital two-photon imaging system for visualising the living bone marrow cavity with high spatiotemporal resolution (figure 1). Using this technique, we have demonstrated that osteoclast precursors migrate under the influence of several chemoattractants and chemorepellants.[8 15 16] The bone marrow is one of the critical developmental sites in the immune system, and bone tissue has a crucial role in the maintenance of its structure. Bone is an active organ, which is continuously remodelled and kept in equilibrium between resorption by osteoclasts and formation by osteoblasts. The disruption of this balance leads to several pathological states, such as osteoporosis, tumour-induced osteolysis and rheumatoid arthritis. In bone-resorptive conditions, osteoclasts are excessively activated and contribute to bone destruction. Osteoclasts are giant multinucleate cells that stem from the monocyte-macrophage lineage of precursor cells. It had remained to be determined where and how the precursors were recruited on the bone surface. Using real-time two-photon microscopy in vivo, we observed migration of osteoclast precursors between the bone marrow cavity and blood vessels, and found that this process depended on C–X–C chemokine ligand 12 (CXCL12), stromal cell-derived factor 1 (SDF-1) and a signalling sphingolipid, suphingosine-1-phospate.

Blood vessels

Following activation within the lymph nodes, immune cells can enter inflamed tissues through blood vessels.[7 17] Neutrophils are innate cell types that are first recruited to the inflamed sites. Intravital microscopy has observed tethering, rolling, crawling and invasion of these cells out of circulation and into the tissues in real time. This recruitment is controlled by several selectin

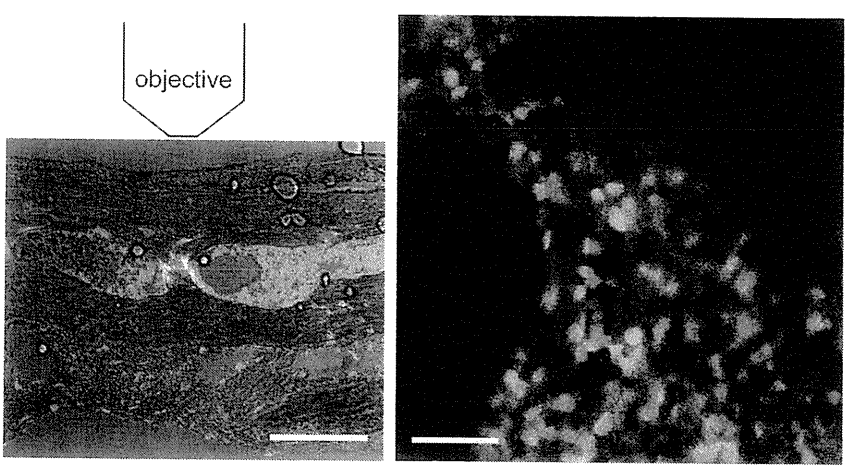

Figure 1 Intravital two-photon imaging of bone marrow. A vertical section of calvaria bone from lysozyme M promoter driven mice expressing enhanced green fluorescent protein (left panel) and intravital imaging of the bone surface using two-photon microscopy (right panel). Blood vessels were visualised by Texas Red-conjugated high molecular dextrans (70 kDa) injected intravenously. Scale bars represent 100 μm (left panel) and 30 μm (right panel), respectively.

Ishii T, Ishii M, *Ann Rheum Dis* 2010;XX:XXX–XXX. doi:10.1136/ard.2010.138156

adhesion molecules, such as P-selectin, E-selectin and L-selectin, as well as integrins. The paths of neutrophil emigration are still controversial. There are two possible routes: a paracellular route, in which neutrophils emigrate at cell–cell junctions, and a transcellular route, in which they emigrate through the endothelial cells.

In addition to neutrophils, monocytes and macrophages also circulate through the vascular system, crawling over the endothelial cell surface.[17] Their attachment depends on interactions between CX_3-chemokine receptor 1 (CX_3CR1) and CX_3-chemokine ligand 1 (CX_3CL1) and between lymphocyte function-associated antigen 1 (LFA1) and intercellular adhesion molecule 1 (ICAM1).

Autoimmune models

Antigen-specific pathogenic T cells have been visualised to migrate through the spinal cord in a murine encephalitis model, EIA.[18] At this site, T cells can be highly motile and arrest antigens upon recognition in the same manner as seen in lymph nodes. In a type I diabetes model using NOD mice, the interaction between antigen-specific T cells and DCs was observed in a draining lymph node.[19] Islet antigen-specific $CD4CD25^-$ T helper cells (Th cells) and regulatory T cells (Treg cells) homed to similar areas of the lymph node and their movement patterns were indistinguishable from each other—that is, they both swarmed and arrested in the presence of antigens. No stable interaction between Th cells and Treg cells was seen, but Treg cells directly interacted with DCs and inhibited Th cell activation via DCs.

FUTURE CHALLENGES

The greatest strength of intravital imaging, the ability to obtain spatiotemporal information in a living body, is not feasible by other methods. This approach has revealed and continues to reveal dynamic features of the immune system including the physiological and pathological process. However, there are several limitations to two-photon microscopy imaging. First, although it has a more extensive penetration depth, it can only image up to 800–1000 μm in soft tissues such as the brain and up to 200 μm in hard tissues such as bone and therefore is not applicable to humans but rather only to small animal models such as mice and rats. Owing to the wide scattering of light by the skin, it is necessary to exteriorise the target organ, and there is a possibility that operative invasion and changes in oxygen concentration and humidity might influence cellular behaviour. To resolve these concerns, technical innovations in fluorochrome and optical systems are expected, including improvements to light emission and resolution.

In the future, intravital microscopy will be applied to both observation and functional analysis. Newly developed fluorescence tools, such as cell cycle indicators,[20] and light-sensing devices, such as light-induced G protein activators, are being introduced.[21] These new approaches are continuing to expand the capacity of in vivo imaging.

CONCLUSIONS

In the past decade, two-photon microscopy has expanded the horizon of intravital imaging. This new technique enables the visualisation of complicated systems of the living body, in which multiple cells are involved. Some technical limitations remain; however, it seems that the range of application is continually increasing.

Competing interests None

Provenance and peer review Not commissioned; externally peer reviewed.

REFERENCES

1. **Denk W,** Strickler JH, Webb WW. Two-photon laser scanning fluorescence microscopy. *Science* 1990;**248**:73–6.
2. **Cahalan MD,** Parker I, Wei SH, *et al.* Two-photon tissue imaging: seeing the immune system in a fresh light. *Nat Rev Immunol* 2002;**2**:872–80.
3. **Germain RN,** Miller MJ, Dustin ML, *et al.* Dynamic imaging of the immune system: progress, pitfalls and promise. *Nat Rev Immunol* 2006;**6**:497–507.
4. **Wang BG,** König K, Halbhuber KJ. Two-photon microscopy of deep intravital tissues and its merits in clinical research. *J Microsc* 2010;**238**:1–20.
5. **Campagnola PJ,** Loew LM. Second-harmonic imaging microscopy for visualizing biomolecular arrays in cells, tissues and organisms. *Nat Biotechnol* 2003;**21**:1356–60.
6. **Miller MJ,** Wei SH, Parker I, *et al.* Two-photon imaging of lymphocyte motility and antigen response in intact lymph node. *Science* 2002;**296**:1869–73.
7. **Garside P,** Brewer JM. Real-time imaging of the cellular interactions underlying tolerance, priming, and responses to infection. *Immunol Rev* 2008;**221**:130–46.
8. **Germain RN,** Bajénoff M, Castellino F, *et al.* Making friends in out-of-the-way places: how cells of the immune system get together and how they conduct their business as revealed by intravital imaging. *Immunol Rev* 2008;**221**:163–81.
9. **Schwickert TA,** Lindquist RL, Shakhar G, *et al.* *In vivo* imaging of germinal centres reveals a dynamic open structure. *Nature* 2007;**446**:83–7.
10. **Bousso P,** Bhakta NR, Lewis RS, *et al.* Dynamics of thymocyte-stromal cell interactions visualized by two-photon microscopy. *Science* 2002;**296**:1876–80.
11. **Le Borgne M,** Ladi E, Dzhagalov I, *et al.* The impact of negative selection on thymocyte migration in the medulla. *Nat Immunol* 2009;**10**:823–30.
12. **Sumen C,** Mempel TR, Mazo IB, *et al.* Intravital microscopy: visualizing immunity in context. *Immunity* 2004;**21**:315–29.
13. **Mazo IB,** Honczarenko M, Leung H, *et al.* Bone marrow is a major reservoir and site of recruitment for central memory CD8+ T cells. *Immunity* 2005;**22**:259–70.
14. **Cavanagh LL,** Bonasio R, Mazo IB, *et al.* Activation of bone marrow-resident memory T cells by circulating, antigen-bearing dendritic cells. *Nat Immunol* 2005;**6**:1029–37.
15. **Ishii M,** Egen JG, Klauschen F, *et al.* Sphingosine-1-phosphate mobilizes osteoclast precursors and regulates bone homeostasis. *Nature* 2009;**458**:524–8.
16. **Klauschen F,** Ishii M, Qi H, *et al.* Quantifying cellular interaction dynamics in 3D fluorescence microscopy data. *Nat Protoc* 2009;**4**:1305–11.
17. **Hickey MJ,** Kubes P. Intravascular immunity: the host-pathogen encounter in blood vessels. *Nat Rev Immunol* 2009;**9**:364–75.
18. **Kawakami N,** Nägerl UV, Odoardi F, *et al.* Live imaging of effector cell trafficking and autoantigen recognition within the unfolding autoimmune encephalomyelitis lesion. *J Exp Med* 2005;**201**:1805–14.
19. **Tang Q,** Adams JY, Tooley AJ, *et al.* Visualizing regulatory T cell control of autoimmune responses in nonobese diabetic mice. *Nat Immunol* 2006;**7**:83–92.
20. **Sakaue-Sawano A,** Kurokawa H, Morimura T, *et al.* Visualizing spatiotemporal dynamics of multicellular cell-cycle progression. *Cell* 2008;**132**:487–98.
21. **Wu YI,** Frey D, Lungu OI, *et al.* A genetically encoded photoactivatable Rac controls the motility of living cells. *Nature* 2009;**461**:104–8.

PDGFRα-positive cells in bone marrow are mobilized by high mobility group box 1 (HMGB1) to regenerate injured epithelia

Katsuto Tamai[a,1], Takehiko Yamazaki[a], Takenao Chino[a], Masaru Ishii[b], Satoru Otsuru[a], Yasushi Kikuchi[a], Shin Iinuma[a], Kotaro Saga[a], Keisuke Nimura[a], Takashi Shimbo[a], Noriko Umegaki[c], Ichiro Katayama[c], Jun-ichi Miyazaki[d], Junji Takeda[e], John A. McGrath[f], Jouni Uitto[g], and Yasufumi Kaneda[a,1]

[a]Division of Gene Therapy Science, and Departments of [c]Dermatology, [d]Nutrition and Physiological Chemistry, and [e]Environmental Medicine, Osaka University Graduate School of Medicine, Osaka 565-0871, Japan; [b]Laboratory of Biological Imaging, WPI-Immunology Frontier Research Center, Osaka University, Osaka 565-0871, Japan; [f]St. John's Institute of Dermatology, King's College London, Guy's Hospital, London SE1 9RT, United Kingdom; and [g]Department of Dermatology and Cutaneous Biology, Jefferson Medical College, Philadelphia, PA 19107

Edited by Darwin J. Prockop, Texas A&M Health Science Center, Temple, TX, and approved March 18, 2011 (received for review November 10, 2010)

The role of bone marrow cells in repairing ectodermal tissue, such as skin epidermis, is not clear. To explore this process further, this study examined a particular form of cutaneous repair, skin grafting. Grafting of full thickness wild-type mouse skin onto mice that had received a green fluorescent protein-bone marrow transplant after whole body irradiation led to an abundance of bone marrow-derived epithelial cells in follicular and interfollicular epidermis that persisted for at least 5 mo. The source of the epithelial progenitors was the nonhematopoietic, platelet-derived growth factor receptor α-positive (Lin^-/$PDGFR\alpha^+$) bone marrow cell population. Skin grafts release high mobility group box 1 (HMGB1) in vitro and in vivo, which can mobilize the Lin^-/$PDGFR\alpha^+$ cells from bone marrow to target the engrafted skin. These data provide unique insight into how skin grafts facilitate tissue repair and identify strategies germane to regenerative medicine for skin and, perhaps, other ectodermal defects or diseases.

epidermolysis bullosa | skin injury | stem cells | keratinocyte | tissue regeneration

Bone marrow (BM) cells contribute a substantial proportion of cells, both inflammatory and noninflammatory, that have roles in tissue homeostasis, repair, and regeneration. Such cells may be derived from either hematopoietic or mesenchymal stem cell populations, and subpopulations thereof can differentiate into both hematopoietic and mesenchymal lineage cells (for review, see refs. 1 and 2).

In skin, studies have shown that BM provides fibroblast-like cells in the dermis (of hematopoietic and mesenchymal lineages) and that the number of these cells increases after skin wounding (3, 4). BM can also generate epithelial cells, i.e., keratinocytes, in the epithelia, although the precise derivations and mechanisms to raise BM-derived keratinocytes are not fully known (3, 5–16). Human/mouse studies involving transplantation of sex-mismatched or genetically tagged BM cells have shown that keratin-positive bone marrow-derived cells can be found in skin epidermis, hair follicles, and sebaceous glands (6, 8, 9, 11, 12, 14, 16), sites that harbor skin stem cell niches (17). Moreover, in humans who have undergone BM transplantation (BMT), donor cells that have differentiated into keratinocytes can be detected in the epidermis for at least 3 y (8).

BM cells also contribute to skin development: Infusion of green fluorescent protein (GFP) BM cells in utero in mice leads to accumulation of a subpopulation of GFP-positive cells in nonwounded skin dermis, particularly in association with developing hair follicles (18). With regard to skin injury, both embryonic and postnatal transplantation of BM cells into mice lacking the skin protein, type VII collagen (Col 7) as well as postnatal studies in mice lacking type XVII collagen, basement membrane components that normally help secure adhesion between the epidermal and dermal skin layers, have demonstrated the capacity of BM to promote skin wound healing and to correct the intrinsic basement membrane defect (18–20). Most recently, a clinical trial of allogeneic whole BMT in humans lacking Col 7 (who have the inherited blistering skin disorder, recessive dystrophic epidermolysis bullosa, RDEB; OMIM226600) (21) has demonstrated that BM cells can repair fragile skin and restore Col 7 expression in skin basement membrane (22).

Collectively, however, these animal and human studies have shown that BM-derived keratinocytes are an extremely rare finding in the epidermis. Indeed, analyses in two different murine models have shown that BM-derived keratinocytes comprise only ≈0.0001–0.0003% of all keratinocytes in the new epidermis (13). The relative scarcity of such cells therefore raises questions about their biological significance. For example, it is not known whether these cells have a physiological role in epithelial regeneration and, if they do, under what circumstances? Moreover, it is not clear which particular cells in BM contribute to the epithelial repair. Furthermore, there is little awareness of the mechanism(s) through which the damaged epithelium signals to invoke mobilization and recruitment of the key BM cells. In this study, we have begun to address these questions, and here report identification of a specific subset of BM cells with epithelial differentiation potential as well as a unique in vivo mechanism through which these cells contribute to epithelial regeneration and maintenance.

Results

We first examined the contribution of BM-derived cells to epithelial regeneration in murine skin wounds. The wounds were created by using a scalpel and involved excision of a piece of full-thickness skin (i.e., including epidermis and dermis) thus creating an ulcer. The mice selected for wounding had received lethal dose irradiation followed by GFP-BMT, thereby allowing us to evaluate the contribution of GFP-BM cells to skin regeneration after injury (Fig. 1*A*). At 4 wk after the injury, GFP-positive keratinocytes were not obvious (Fig. 1*B*), indicating a minimal, if any, contribution of BM cells to epithelial regeneration, findings consistent with previous data (13). We then used the same

Author contributions: K.T. designed research; K.T., T.Y., T.C., M.I., S.O., Y. Kikuchi, S.I., K.S., K.N., T.S., and N.U. performed research; J.-i.M. and J.T. contributed new reagents/analytic tools; K.T., I.K., and Y. Kaneda analyzed data; and K.T., J.A.M., J.U., and Y. Kaneda wrote the paper.

Conflict of interest statement: K.T., T.Y., and Y. Kaneda have filed patents relating to the use of HMGB1 for bone marrow cell mobilization and recruitment to damaged tissue. These individuals also hold stock in Genomix plc, a bio-tech company involved in HMGB1 translational research.

This article is a PNAS Direct Submission.

Freely available online through the PNAS open access option.

[1]To whom correspondence may be addressed. E-mail: tamai@gts.med.osaka-u.ac.jp or kaneday@gts.med.osaka-u.ac.jp.

This article contains supporting information online at www.pnas.org/lookup/suppl/doi:10.1073/pnas.1016753108/-/DCSupplemental.

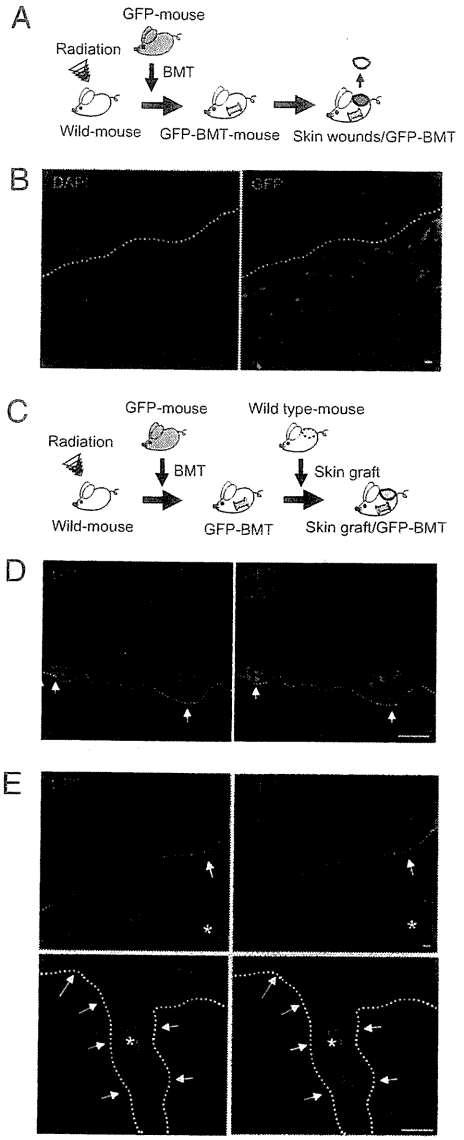

Fig. 1. BM-derived cells contribute to epidermal and follicular renewal in skin grafts, but not in skin wounds. (*A*) Schematic outlining details of the skin wound model on GFP-BMT mice. (*B*) Confocal-laser microscopy of skin sections from the reepithelialized wounds. Green fluorescence in the dermis represents BM-derived cells. Note that there is no GFP fluorescence within the regenerated epithelia. (*C*) Schematic outlining details of the skin engraftment of GFP-BMT mice. (*D*) Confocal-laser microscopy of skin sections from the 4-wk skin graft. Green fluorescence in the epidermis and the dermis represent BM-derived cells. Arrows indicate EPU-like structures that are composed of BM-derived epithelial cells emanating from the basal layer (white arrows) within the epidermis to the horny layer (red arrowheads). (*E*) Confocal-laser microscopy pictures of skin sections from the 5-mo skin graft. Green fluorescence in the epidermis, the hair follicles, and the dermis represent BM-derived cells. Arrows in *Upper* indicate sustained BM-derived epithelial cells emanating from the basal layer (white arrows) to the horny layer (red arrows). White arrows in *Lower* indicate sustained BM-derived follicular cells. Note that hair shafts show nonspecific auto-fluorescence (asterisks). White dotted lines indicate the dermal-epidermal and dermal-follicular junctions. (Scale bars: 50 μm.)

mouse model to examine a different form of skin repair, skin grafting, to further explore the potential contribution of BM cells (Fig. 1*C*). Surprisingly, we noted that significant numbers of GFP-positive cells expressing skin-specific keratin 5 formed epidermal proliferative unit (EPU)-like clusters in the epidermis of the skin graft in biopsies taken 4 wk after the engraftment (Fig. 1*D* and Fig. S1*A*). Furthermore, the BM-derived GFP-positive keratinocytes were maintained in the epidermis and hair follicles 5 mo after the engraftment (Fig. 1*E* and Fig. S1*B*). Given that mouse epidermis is renewed every 2–3 wk by epithelial stem cell-derived keratinocytes, those long-residing GFP BM-derived epithelial cells in the 5-mo-old graft are likely to contain epithelial progenitor/stem cells.

To assess whether the BM-derived epidermal cells might have functional significance, we then searched for BM-derived cells in the skin of Col 7-null mice engrafted onto the GFP-BMT mice (Fig. 2*A*). Because these mice have complete detachment of the epidermis after birth due to extensive skin and mucous membrane fragility (Fig. 2*A*) (23), we anticipated a potentially greater contribution of BM-derived cells in the regenerating epithelia of the engrafted Col 7-null mouse skin. The engrafted Col 7-null mouse skin initially showed extensive subepidermal detachment, similar to the skin pathology seen in human patients with RDEB (21). At 4 wk after the engraftment, we noted an even greater contribution of GFP-positive cells expressing keratinocyte-specific keratins in the regenerating epidermis and hair follicles of the engrafted Col 7-null mouse skin (Fig. 2 *B–D* and Fig. S2). Moreover, new Col 7 protein was present at the cutaneous basement membrane zone in the engrafted Col 7-null mouse skin (Fig. 2*E*). Notably, Col 7 labeling was maximal in the basement membrane adjacent to GFP-BM–derived epithelial cells. Evidence for BM-derived epithelial cells was further confirmed by demonstration of GFP-positive individual keratinocytes from the grafted skin by means of both flow cytometric analysis and cell culture (Fig. 2 *F* and *G*).

Collectively, these data showed that a subpopulation of BM cells contribute to epithelial regeneration and maintenance in these murine skin graft models. Analyses of sex chromatin numbers and fusion-dependent enhanced GFP expression in BM-derived epithelial cells in the grafted skin did not show any evidence for cell fusion, suggesting differentiation of the BM-derived cells as the likely mechanism for raising BM-derived keratinocytes in the skin graft (Figs. S3 and S4). Reverse wild-type BMT in a GFP mouse, followed by engrafting Col 7-null mouse skin onto the back of this mouse, excluded other possible extrinsic sources of keratinocytes in the skin graft besides the BM (Fig. S5).

We then investigated the subpopulation of BM cells that has the potential for epithelial differentiation. Recent studies have shown that the PDGFRα-positive nonhematopoietic BM cell population contains ectoderm-derived mesenchymal stem cells (MSCs) (24–26), indicating that perhaps PDGFRα$^+$ BM cells might be a putative source of BM-derived keratinocytes in the skin graft. To test this hypothesis, we examined BM from a heterozygous knock-in mouse in which a histone H2B-GFP fusion gene was inserted into the locus of the PDGFRα gene (PDGFRα-H2BGFP mouse); this knock-in results in accumulation of GFP fluorescence within the nuclei of PDGFRα-expressing cells. We found that the PDGFRα$^+$ BM cells were exclusively enriched in the Lineage-negative (Lin$^-$) cell population from the knock-in mouse BM (Fig. S6) and that the Lin$^-$ population provided proliferating PDGFRα$^+$ fibroblastic cells in culture (Fig. 3*A*). Lin$^-$ indicates negativity for the cell surface antigens CD5, B220, CD11b, Gr-1, 7–4, and Ter-119 and excludes mature hematopoietic cells, such as T cells, B cells, monocytes/macrophages, granulocytes, and erythrocytes/their committed precursors from BM. Flow cytometric analysis indicated that the Lin$^-$ and PDGFRα$^+$ (Lin$^-$/PDGFRα$^+$) cells were independent from the Lin$^-$/c-kit$^+$ cell population, which includes a hematopoietic stem cell pool (Lin$^-$/c-kit$^+$/Sca-1$^+$) in BM (Fig. 3*B* and Fig. S7). We found that Lin$^-$ cell populations collectively accounted for ≈5.6% of the total number of BM cells (Fig. 3*B*). The Lin$^-$/PDGFRα$^-$/c-kit$^+$ and Lin$^-$/PDGFRα$^-$/c-kit$^-$ BM cells comprised ≈2.28% and ≈3.11% of total BM cells, respectively. We observed that the Lin$^-$/PDGFRα$^+$ BM cells (≈0.22% of the total BM cells) could exclusively generate BM-derived epithelial cells expressing keratin 5 in culture after supplementation with skin soaked buffer (SSB),

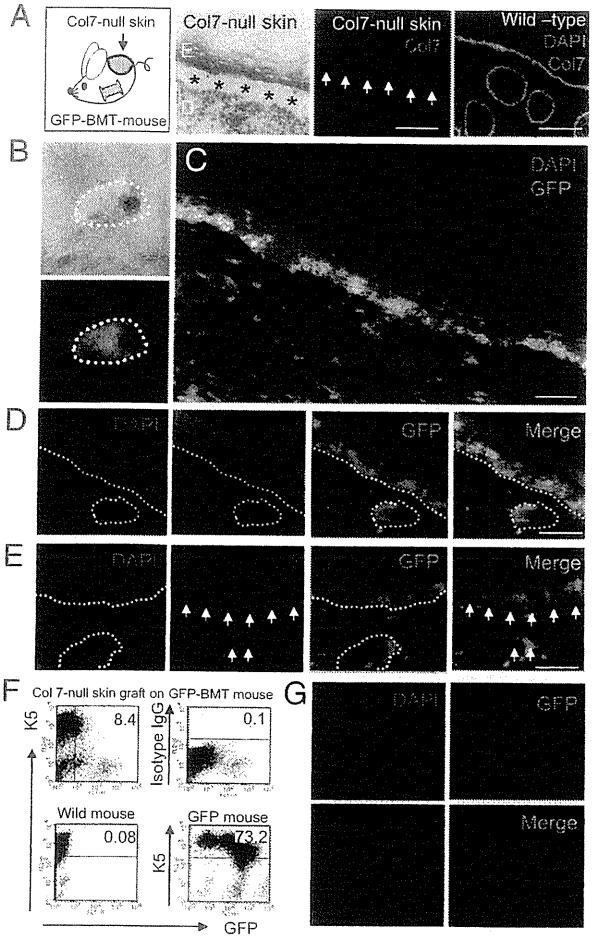

Fig. 2. BM cells substantially contribute to the repair of grafted Col 7-null epidermis. (*A*) Schematic picture of the Col 7-null skin engraftment on GFP-BMT mice (*Left*); hematoxylin-eosin staining of Col 7-null mouse skin (*Left Center*). Asterisks indicate separation of the epidermis (*E*) from the dermis (*D*); Col 7 immunostaining in the Col 7-null skin (*Right Center*). (*Right*) Arrows indicate dermal-epidermal junction, Col 7 staining of wild-type mouse skin. Green color indicates Col 7 staining. (*B*) Accumulation of GFP fluorescence (*Lower*) within the region of the Col 7-null skin graft (*Upper*). The white dotted line indicates the margins of the skin graft. (*C* and *D*) Confocal-laser microscopy pictures of sections from the Col 7-null mouse skin that had been surgically grafted. Blue color indicates DAPI staining. Green fluorescence in the epidermis and the dermis represents BM-derived cells. Red labeling indicates keratin 5 (K5; *C*) or keratin 10 (K10; *D*) immunofluorescence. Yellow color image represents BM-derived cells that express both GFP (green) and K5 (red; *C*) or K10 (red; *D*). (*E*) Col 7 expression in grafted Col 7-null mouse skin. White dotted lines indicate dermal-epidermal and dermal-follicular junctions. White arrows indicate immunofluorescence for Col 7 (red) at the basement membrane zone. (Scale bars: 50 μm.) (*F*) Flow cytometric analysis for K5 and GFP in the epidermal cell suspension of Col 7-null skin engrafted onto a GFP-BMT mouse (*Upper Left*), wild-type mouse skin (*Lower Left*), and the GFP-transgenic mouse skin (*Lower Right*). *Upper Right* shows isotype control for K5 in the epidermis of the grafted Col 7-null skin. (*G*) Confocal-laser micrographs of cultured BM-derived epithelial cells isolated from the epidermis of the Col 7-null skin graft labeled with GFP or K5.

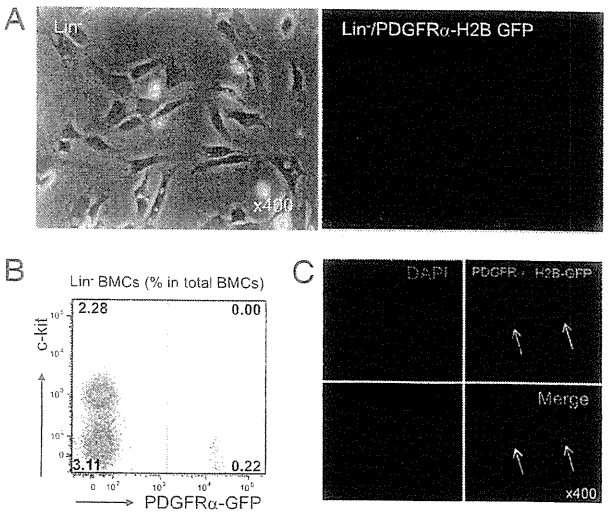

Fig. 3. Characterization of BM cells of the PDGFRα knock-in mouse demonstrates that PDGFRα$^+$ subpopulation give rise to epithelial progenitors. (*A*) Phase-contrast (*Left*) and GFP-fluorescent (*Right*) micrographs of the Lin$^-$ BM cells in culture. All adherent and proliferating Lin$^-$ cells were positive with PDGFRα-GFP labeling in their nuclei. (*B*) Flow cytometry analysis for PDGFRα-GFP and c-kit expression on the Lin$^-$ cells in total BM cells of the PDGFRα knock-in mice. The number (%) in the chart represents the population of each fraction in the total number of BM cells. Note that there is no population in the PDGFRα-positive and c-kit-positive fraction (upper right corner) in BM. (*C*) Confocal-laser micrographs of cultured bone marrow cells (BMCs) from a heterozygous knock-in mouse with a histone H2B-GFP fusion gene inserted into the PDGFRα gene locus. PDGFRα promoter-dependent H2B-GFP expression was noted by accumulation of GFP fluorescence in the nuclei (PDGFRα/H2B-GFP, indicated by white arrows; *Upper Right*) of cells expressing K5 (*Lower Left*).

in which excised newborn mouse skin had been soaked in phosphate buffer saline (PBS) for 24 h (Fig. 3*C* and Fig. S8). The Lin$^-$/PDGFRα$^-$ cell population also contained adherent and proliferative cells in culture, but none of these cells showed differentiation into keratin 5-positive keratinocytes with SSB supplementation (Fig. S8). These data suggest that the BM-derived keratinocytes are not of hematopoietic origin, but instead are derived from a specific subpopulation of Lin$^-$/PDGFRα$^+$ BM cells. In this context, additional flow cytometry analysis of the Lin$^-$/PDGFRα$^+$ BM cells did not show expression of CD146 or CD271 (Fig. S9), both of which are established markers of human BM MSCs (27), indicating different cell surface molecule profiles for human BM MSCs and mouse Lin$^-$/PDGFRα$^+$ BM cells.

We then investigated the mechanism through which the transplanted skin graft is able to recruit Lin$^-$/PDGFRα$^+$ cells from the BM. First, we established a Boyden chamber migration assay to demonstrate that Lin$^-$/PDGFRα$^+$ BM cells migrate toward one or more chemoattractants in SSB (Fig. 4*A*). We then assessed which molecules in the SSB have the capacity to induce migration of Lin$^-$/PDGFRα$^+$ BM cells. We noted that a heparin-binding fraction of SSB was able to induce robust migration of the Lin$^-$/PDGFRα$^+$ BM cells (Fig. 4*B*). This finding supports the notion that the excised skin graft can release heparin-binding molecules capable of attracting these particular BM cells. To find the precise molecules involved, we fractionated SSB by heparin-affinity chromatography and obtained several fractions with strong activity for inducing Lin$^-$/PDGFRα$^+$ BM cell migration (Fig. S10). Some fractions had strong cell-migrating activity but comparatively less protein expression: These fractions were then subjected to SDS/PAGE analysis (Fig. 4*C*). Three prominent silver-stained proteins were observed in the gel, which were then further analyzed by liquid chromatography/tandem mass spectrometry. They were identified as nucleolin, anti-thrombin III (AT-III), and high mobility group box 1 (HMGB1) (Fig. 4*C*). Nucleolin is a eukaryotic nucleolar phosphoprotein that is involved in the synthesis and maturation of ribosomes in nucleoli (28). AT-III is a well-characterized anticoagulant molecule generated in the liver, and which exists in blood plasma (29). HMGB1, also known as amphoterin, is a nuclear protein that can regulate chromatin structure and gene expression (30). It is also released from necrotic cells and some apoptotic cells and acts

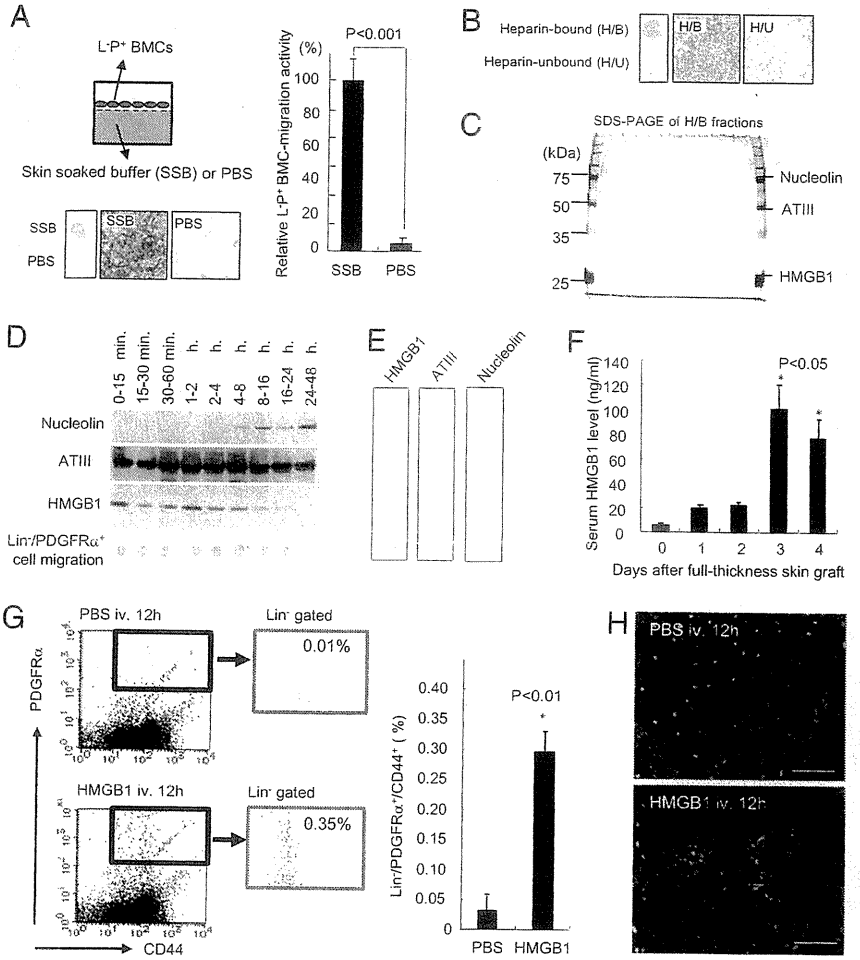

Fig. 4. Elevation of HMGB1 in serum is induced by skin grafting and mobilizes Lin⁻/PDGFRα⁺ cells from BM. (*A*) Schematic illustration of the Boyden chamber approach to assess migration of the Lin⁻/PDGFRα⁺ cells to SSB or PBS. The actual and relative migration of these cells to both buffers is shown. (*B*) Assessment of Lin⁻/PDGFRα⁺ cells migration to heparin-bound (H/B) or unbound (H/U) fractions of the SSB. (*C*) SDS/PAGE of H/B SSB fractions with Lin⁻/PDGFRα⁺ cell migration activity. Results of liquid chromatography-tandem mass spectrometry for three major proteins in the gel are noted on the right. (*D*) Western blot against nucleolin, AT-III, and HMGB1 in the SSB obtained at sequential time periods. The lowest blot shows Lin⁻/PDGFRα⁺ cell migration activities in each SSB. (*E*) Lin⁻/PDGFRα⁺ cell migration assay in a Boyden chamber with recombinant HMGB1, AT-III, and nucleolin. (*F*) HMGB1 levels in mouse sera after full-thickness skin grafting with newborn wild-type mouse skin. Asterisks (*) indicate statistical significance vs. Day 0 ($P < 0.05$, $n = 4$). (*G*) Flow cytometric analyses of Lin⁻/PDGFRα⁺/CD44⁺ cells of peripheral blood mononuclear cells of mice 12 h after systemic administration of HMGB1 (10 μg in 400 μL of PBS) or PBS (400 μL). Asterisk (*) represents statistical significance ($P < 0.01$, $n = 4$). (*H*) Intravital two-photon imaging of the calvaria BM in PDGFRα-H2BGFP mice 12 h after systemic administration of PBS (400 μL; *Left*) or HMGB1 (10 μg in 400 μL of PBS; *Right*) via the tail vein. Green color, GFP expressed under the promoter of PDGFRα; red color, BM microvasculature visualized by i.v. injection of 70-kDa dextran-conjugated Texas Red. (Scale bar: 50 μm.)

as an inflammatory regulator. Other studies, however, have indicated that HMGB1 may also act as a local chemo-attractant for various hematopoietic and nonhematopoietic cells that can regulate tissue remodeling (31).

The next objective was to determine the time course for release of the proteins from excised skin graft into the buffer (Fig. 4*D*). Of note, both HMGB1 and AT-III were rapidly released within a few minutes into the SSB fraction that demonstrated strong chemoattractant activity for Lin⁻/PDGFRα⁺ BM cells. AT-III secretion continued at similar levels for at least 48 h, whereas HMGB1 release gradually declined after ≈8 h—a time course that paralleled the chemoattraction findings. With regard to nucleolin, its presence in the SSB only started 2 h after incubation, possibly reflecting the consequences of necrosis in the excised skin. To evaluate the chemoattractant properties, we expressed mouse HMGB1 in HEK293 cells and compared the in vitro activity of the purified recombinant protein to induce Lin⁻/PDGFRα⁺ BM cell migration. Recombinant AT-III and nucleolin were also assessed, but cell migration assays demonstrated that only HMGB1 could induce migration of these particular BM cells (Fig. 4*E*). We also explored the nature of the receptor on Lin⁻/PDGFRα⁺ BM cells relevant to the cell migration and excluded a role for two known receptors that can mediate the extracellular cytokine effects of HMGB1, the receptor for advanced glycation endproduct (RAGE) and toll-like receptor (TLR) 4 (32–34) (see *SI Results and Discussion* and Fig. S11 for details).

Next, we explored the source of HMGB1 in the grafted skin. Immunofluorescent microscopy analysis of HMGB1 protein in the skin graft showed abundant staining in the epidermis and much less in the dermis, reflecting the higher cellularity in the epidermis (Fig. S12). We then analyzed Col 7-null mouse skin for HMGB1 release and noted that the detached epithelia (blister roofs) released significant amounts of HMGB1 after soaking in PBS (Fig. S13 *A* and *B*). These observations suggest that the epithelial tissue in the skin graft could be a significant source of HMGB1 in vivo. Further support for damaged epithelium as a source of HMGB1 was demonstrated by finding elevated HMGB1 in freshly generated subepidermal blister fluid of human subjects with RDEB ($n = 3$) (Fig. S13*C*). We then investigated the systemic effects of HMGB1 after skin injury. We first measured HMGB1 levels in the sera of mice that had received a skin graft of wild-type newborn mouse skin (Fig. 4*F*). We observed a marked increase in HMGB1 serum levels 3 d after grafting. Of note, however, no increase in serum HMGB1 was noted in mice with full thickness wounds but no skin graft (Fig. S13*D*), suggesting that the transplanted epithelial tissue is likely to be the source of the elevated HMGB1 in the sera. We also detected ≈60-fold higher levels of HMGB1 in the sera of individuals with RDEB ($n = 3$) compared with similarly aged normal control subjects ($n = 3$) (Fig. S13*E*). These observations led us to hypothesize that systemic elevation of HMGB1 in the blood might positively induce recruitment of Lin⁻/PDGFRα⁺ cells from BM to raise BM-derived keratinocytes (as well as fibroblasts) in the regenerating injured skin, and that this might be one mechanism through which the practice of skin grafting achieves its clinical goals.

To confirm this hypothesis, we systemically administered recombinant HMGB1 at levels similar to that seen in the sera of skin grafted mice to wild-type mice. We observed that this action could mobilize Lin⁻/PDGFRα⁺ BM cells into the blood circulation (Fig. 4*G*). Lower doses of HMGB1 failed to mobilize

these cells (Fig. S14). We noted no local or systemic inflammation or other potentially adverse effects in the mice, despite the high doses of systemic HMGB1 administered (Fig. S15). To further investigate the mechanics of this mobilization by HMGB1 in vivo, we performed intravital two-photon imaging of calvaria BM in living PDGFRα-H2BGFP mice. This experiment showed that HMGB1 could mobilize PDGFRα-positive cells, allowing them to congregate around blood vessels and, thereby, allow egress into the circulation in vivo (Fig. 4*H*).

To confirm that the mobilized BM-derived PDGFRα$^+$ circulating cells provide the epithelial cells in vivo, we combined FACS-sorted PDGFRα$^+$/GFP$^+$ BM cells with wild-type PDGFRα$^-$ BM cells and transplanted these cells to lethally irradiated mice, which then received skin grafts of Col 7-null mouse skin (Fig. 5*A*). Very few cells were GFP-positive in the peripheral blood mononuclear cell populations of the PDGFRα$^+$/GFP$^+$ BM transplanted mice (Fig. 5*B*). However, those GFP-positive circulating cells that originated from the transplanted PDGFRα$^+$ BM cells had adherent and proliferative capacities in culture (Fig. 5*B*). Four weeks after the Col 7-null skin engraftment, multiple foci of GFP-positive cells expressing keratin 5 were observed in the epithelia of the engrafted skin (Fig. 5*C*), suggesting that the BM-derived PDGFRα$^+$ circulating cells contain a population that can differentiate into epithelial cells in the skin graft.

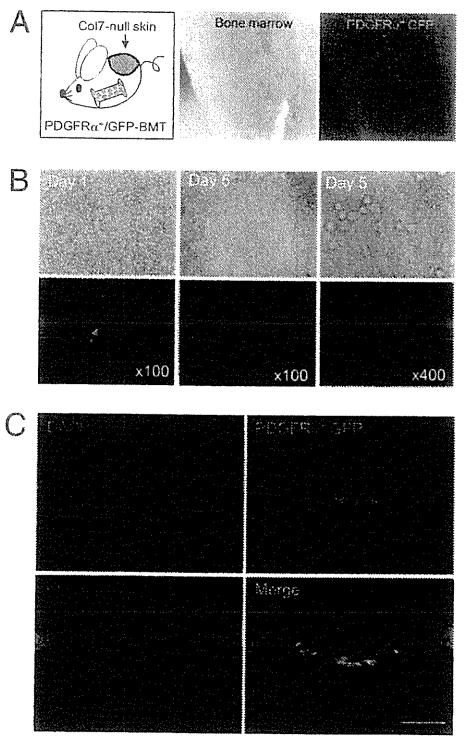

Fig. 5. Mobilized Lin$^-$/PDGFRα$^+$ BM-derived cells in circulation contribute to epithelial regeneration of the skin graft in vivo. (*A*) Schematic illustration showing Col 7-null skin graft on a mouse transplanted with PDGFRα-positive/GFP-BM cells (*Left*); bright field (*Center*) and dark field (*Right*) stereomicroscopic pictures of femoral BM in a PDGFRα$^+$/GFP-BMT mouse. Green fluorescence indicates PDGFRα$^+$/GFP-BM cells. (*B*) Bright field (*Upper*) and dark field (*Lower*) fluorescent microscopic pictures of cultured peripheral blood mononuclear cells that were obtained from the PDGFRα$^+$/GFP-BMT mouse engrafted with Col 7-null skin. (*Left*) A single PDGFRα$^+$/GFP-BM-derived cell in culture (Day 1). (*Center*) Proliferation of the single PDGFRα$^+$/GFP-BM-derived cell in culture (Day 5). (*Right*) Dividing adherent cells indicated in the white lined box in *Lower Center*. (*C*) Confocal-laser microscopic pictures of a section of grafted Col7-null skin onto a PDGFRα$^+$/GFP-BMT mouse. GFP fluorescence was merged with the red immunofluorescence of K5 to provide the yellow color. DAPI staining (*Upper Left*), GFP fluorescence (*Upper Right*), K5 staining (*Lower Left*), and a merged image (*Lower Right*). (Scale bar: 50 μm.)

Discussion

This work clearly demonstrates that Lin$^-$/PDGFRα$^+$ cells from BM significantly contribute to the regeneration of the epidermis after skin grafting in vivo, and that one biological repair mechanism involves the key cells being mobilized in response to elevated HMGB1 levels in serum, the source of which is the skin graft. The observation that tissue damage can recruit BM stromal cells for tissue repair is well-established (35), but here we have defined a subpopulation of cells that have the capacity to repair skin, including epidermis. The Lin$^-$/PDGFRα$^+$ BM cell marker profile is not unique to one particular cell population, and our data suggest that it is shared by ≈1 in 450 BM cells. PDGFRα is not expressed by hematopoietic stem cells but by MSCs in bone marrow that can give rise to mesenchymal lineage cells as well as neuroepithelial and neural crest lineage cells (24–26), suggesting that the Lin$^-$/PDGFRα$^+$ BM cells contain an MSC fraction (discussed further in *SI Results and Discussion*).

Our study has shown that in situations in which there is significant damage to the epidermis, such as Col 7 deficiency leading to subepidermal blistering, at least some of the Lin$^-$/PDGFRα$^+$ cells have the plasticity to become BM-derived epithelial progenitors, to generate and sustain new keratinocytes, and to correct the intrinsic lack of Col 7. Moreover, we have identified HMGB1 as a specific factor involved in Lin$^-$/PDGFRα$^+$ BM cell responses. Our data indicate that HMGB1, which is rapidly released from the detached or blistered Col 7-deficient epithelia, can mobilize Lin$^-$/PDGFRα$^+$ BM cells into the circulation and accelerate regeneration of the skin by recruiting these cells to raise BM-derived epithelial cells and BM-derived mesenchymal cells in the epidermis and dermis of Col 7-null skin, respectively.

HMGB1 is a highly conserved, abundant, and ubiquitously expressed 30-kDa nonhistone protein with diverse biologic functions (36, 37). With regards to human and murine HMGB1, only 2 of 215 amino acids show species differences (>99% identical) and both reside in the C-terminal region outside of the known receptor- and DNA-binding motifs (38, 39). HMGB1 can act as a mobile and dynamic nucleo-cytoplasmic protein influencing multiple processes in chromatin such as transcription, replication, recombination, and DNA repair (39, 40), but HMGB1 can also be secreted into the extracellular milieu as a signaling molecule when cells are stressed (41). HMGB1 can bind exogenous and endogenous agents such as endotoxin, microbial DNA, and nucleosomes, and induces adaptive and innate immune responses via TLR2/4/9 followed by NF-κB activation (42, 43), contributing to inflammation, autoimmune dysregulation, and carcinogenesis. However, purified recombinant HMGB1 has little, if any, proinflammatory activity (44). Indeed, free HMGB1, that is unbound to endogenous/exogenous inflammatory factors, is able to suppress inflammatory reactions in noninjured tissues by inhibiting TLR-mediated NF-κB signaling (33). Biologically, HMGB1 can be regarded as a critical factor for maintaining tissue homeostasis in cleaning damaged/infected tissues (i.e., promoting intralesional inflammation), but also in protecting surrounding noninjured tissues (i.e., suppressing inflammation), and accelerating regeneration of damaged tissues by mobilizing and recruiting specific BM cells, that include epithelial progenitors when there is extensive epithelial injury, such as in Col 7-deficient RDEB skin.

The concept that a particular threshold concentration of HMGB1 in serum is relevant to mobilizing Lin$^-$/PDGFRα$^+$ BM cells and targeting them to damaged tissue also offers unique possibilities to augment a variety of other tissue repair mechanisms. It is likely that, in several other situations, systemic administration of HMGB1 to achieve serum levels similar to those observed in RDEB could be used as a therapeutic strategy to recruit stem/progenitor cells to accelerate regeneration of damaged tissue. Precisely which tissues might benefit from HMGB1-induced mobilization of Lin$^-$/PDGFRα$^+$ BM cells remains to be determined. What has also not been determined thus far are the dynamics of both the release of the Lin$^-$/PDGFRα$^+$ cells from the BM and the events that promote recruitment and migration within the target tissue and the other potential local microenvironment-

induced and biochemical processes that contribute to improved wound healing (35) (discussed further in *SI Materials and Methods*). Nevertheless, we believe our data represent a significant advance in identifying a direction for potentially bringing stem/progenitor cell regenerative medicine to a broader clinical arena.

Materials and Methods

BMT. BM cells were isolated under sterile conditions from 8- to 10-wk-old male C57BL/6 transgenic mice that ubiquitously expressed enhanced green fluorescent protein (GFP). Recipients were 8- to 10-wk-old female C57BL/6 mice that were lethally irradiated with 10 Gy of X-rays, and each irradiated recipient received 5×10^6 BM cells from GFP transgenic mice kindly provided by Masaru Okabe (Osaka University). Experiments were performed on the BMT mice at least 6 wk after the BMT.

Mouse Skin Transplantation. Full-thickness skin from wild-type and Col 7-null newborn mice (graft size $\approx 2 \times 2$ cm) was carefully isolated by excision after the mice had been euthanized under systemic anesthesia, and engrafted onto the backs of the GFP-BMT mice, wild-type BMT mice, and K5-Cre-GFP-BMT mice, with grafting just above the muscular fascia.

Immunofluorescent Microscopy Analysis. The engrafted skins were removed, fixed with 2% paraformaldehyde, and subjected to immunofluorescent analysis. The excised skins were embedded in Tissue-Tec OCT Compound (Sakura Finetek), frozen on dry ice, and stored at −20 °C. For immunofluorescence staining, 6-μm-thick sections were labeled with rabbit polyclonal anti-mouse antibodies. Subsequently, sections were stained with goat anti-rabbit IgG secondary antibody.

Cell-Migration Assay. Chemokinetic migration of $Lin^-/PDGFR\alpha^+$ cells was assayed by using a modified Boyden chamber. In brief, 1.0 μg of HMGB1 in 27 μL of DMEM was added in the lower chambers, and 10^6 cells/mL of $Lin^-/PDGFR\alpha^+$ cells suspended in 50 μL of DMEM containing 10% FBS were added to the upper chamber. The cells on the lower side of the membrane were stained with Diff-Quick (Sysmex).

ACKNOWLEDGMENTS. This work was supported by the following grants: a grant from the Northern Osaka (Saito) Biomedical Knowledge-Based Cluster Creation Project; Special Coordination Funds for Promoting Science and a Grant-in-Aid for Scientific Research from the Ministry of Education, Culture, Sports, Science and Technology of Japan; and a Health and Labour Sciences Research Grant (Research of Intractable Diseases) from the Ministry of Health, Labour and Welfare of Japan.

1. Orkin SH, Zon LI (2008) Hematopoiesis: An evolving paradigm for stem cell biology. *Cell* 132:631–644.
2. Prockop DJ (2009) Repair of tissues by adult stem/progenitor cells (MSCs): Controversies, myths, and changing paradigms. *Mol Ther* 17:939–946.
3. Fathke C, et al. (2004) Contribution of bone marrow-derived cells to skin: Collagen deposition and wound repair. *Stem Cells* 22:812–822.
4. Ishii G, et al. (2005) In vivo characterization of bone marrow-derived fibroblasts recruited into fibrotic lesions. *Stem Cells* 23:699–706.
5. Wu Y, Zhao RC, Tredget EE (2010) Concise review: Bone marrow-derived stem/progenitor cells in cutaneous repair and regeneration. *Stem Cells* 28:905–915.
6. Krause DS, et al. (2001) Multi-organ, multi-lineage engraftment by a single bone marrow-derived stem cell. *Cell* 105:369–377.
7. Hematti P, et al. (2002) Absence of donor-derived keratinocyte stem cells in skin tissues cultured from patients after mobilized peripheral blood hematopoietic stem cell transplantation. *Exp Hematol* 30:943–949.
8. Körbling M, et al. (2002) Hepatocytes and epithelial cells of donor origin in recipients of peripheral-blood stem cells. *N Engl J Med* 346:738–746.
9. Badiavas EV, Falanga V (2003) Treatment of chronic wounds with bone marrow-derived cells. *Arch Dermatol* 139:510–516.
10. Badiavas EV, Abedi M, Butmarc J, Falanga V, Quesenberry P (2003) Participation of bone marrow derived cells in cutaneous wound healing. *J Cell Physiol* 196:245–250.
11. Kataoka K, et al. (2003) Participation of adult mouse bone marrow cells in reconstitution of skin. *Am J Pathol* 163:1227–1231.
12. Borue X, et al. (2004) Bone marrow-derived cells contribute to epithelial engraftment during wound healing. *Am J Pathol* 165:1767–1772.
13. Fan Q, et al. (2006) Bone marrow-derived keratinocytes are not detected in normal skin and only rarely detected in wounded skin in two different murine models. *Exp Hematol* 34:672–679.
14. Inokuma D, et al. (2006) CTACK/CCL27 accelerates skin regeneration via accumulation of bone marrow-derived keratinocytes. *Stem Cells* 24:2810–2816.
15. Rovó A, Gratwohl A (2008) Plasticity after allogeneic hematopoietic stem cell transplantation. *Biol Chem* 389:825–836.
16. Sasaki M, et al. (2008) Mesenchymal stem cells are recruited into wounded skin and contribute to wound repair by transdifferentiation into multiple skin cell type. *J Immunol* 180:2581–2587.
17. Fuchs E, Horsley V (2008) More than one way to skin . . .. *Genes Dev* 22:976–985.
18. Chino T, et al. (2008) Bone marrow cell transfer into fetal circulation can ameliorate genetic skin diseases by providing fibroblasts to the skin and inducing immune tolerance. *Am J Pathol* 173:803–814.
19. Tolar J, et al. (2009) Amelioration of epidermolysis bullosa by transfer of wild-type bone marrow cells. *Blood* 113:1167–1174.
20. Fujita Y, et al. (2010) Bone marrow transplantation restores epidermal basement membrane protein expression and rescues epidermolysis bullosa model mice. *Proc Natl Acad Sci USA* 107:14345–14350.
21. Fine JD, et al. (2008) The classification of inherited epidermolysis bullosa (EB): Report of the Third International Consensus Meeting on Diagnosis and Classification of EB. *J Am Acad Dermatol* 58:931–950.
22. Wagner JE, et al. (2010) Bone marrow transplantation for recessive dystrophic epidermolysis bullosa. *N Engl J Med* 363:629–639, and erratum (2010) 363:1383.
23. Heinonen S, et al. (1999) Targeted inactivation of the type VII collagen gene (Col7a1) in mice results in severe blistering phenotype: A model for recessive dystrophic epidermolysis bullosa. *J Cell Sci* 112:3641–3648.
24. Takashima Y, et al. (2007) Neuroepithelial cells supply an initial transient wave of MSC differentiation. *Cell* 129:1377–1388.
25. Morikawa S, et al. (2009) Prospective identification, isolation, and systemic transplantation of multipotent mesenchymal stem cells in murine bone marrow. *J Exp Med* 206:2483–2496.
26. Morikawa S, et al. (2009) Development of mesenchymal stem cells partially originate from the neural crest. *Biochem Biophys Res Commun* 379:1114–1119.
27. Bühring HJ, et al. (2009) Phenotypic characterization of distinct human bone marrow-derived MSC subsets. *Ann N Y Acad Sci* 1176:124–134.
28. Mongelard F, Bouvet P (2007) Nucleolin: A multiFACeTed protein. *Trends Cell Biol* 17:80–86.
29. Quinsey NS, Greedy AL, Bottomley SP, Whisstock JC, Pike RN (2004) Antithrombin: In control of coagulation. *Int J Biochem Cell Biol* 36:386–389.
30. Harris HE, Raucci A (2006) Alarmin(g) news about danger: Workshop on innate danger signals and HMGB1. *EMBO Rep* 7:774–778.
31. Palumbo R, Bianchi ME (2004) High mobility group box 1 protein, a cue for stem cell recruitment. *Biochem Pharmacol* 68:1165–1170.
32. Riuzzi F, Sorci G, Donato R (2006) The amphoterin (HMGB1)/receptor for advanced glycation end products (RAGE) pair modulates myoblast proliferation, apoptosis, adhesiveness, migration, and invasiveness. Functional inactivation of RAGE in L6 myoblasts results in tumor formation in vivo. *J Biol Chem* 281:8242–8253.
33. Chen GY, Tang J, Zheng P, Liu Y (2009) CD24 and Siglec-10 selectively repress tissue damage-induced immune responses. *Science* 323:1722–1725.
34. Maroso M, et al. (2010) Toll-like receptor 4 and high-mobility group box-1 are involved in ictogenesis and can be targeted to reduce seizures. *Nat Med* 16:413–419.
35. Phinney DG, Prockop DJ (2007) Concise review: Mesenchymal stem/multipotent stromal cells: the state of transdifferentiation and modes of tissue repair—current views. *Stem Cells* 25:2896–2902.
36. Rauvala H, Rouhiainen A (2010) Physiological and pathophysiological outcomes of the interactions of HMGB1 with cell surface receptors. *Biochim Biophys Acta* 1799:164–170.
37. Sims GP, Rowe DC, Rietdijk ST, Herbst R, Coyle AJ (2010) HMGB1 and RAGE in inflammation and cancer. *Annu Rev Immunol* 28:367–388.
38. Baxevanis AD, Landsman D (1995) The HMG-1 box protein family: Classification and functional relationships. *Nucleic Acids Res* 23:1604–1613.
39. Stros M (2010) HMGB proteins: Interactions with DNA and chromatin. *Biochim Biophys Acta* 1799:101–113.
40. Liu Y, Prasad R, Wilson SH (2010) HMGB1: Roles in base excision repair and related function. *Biochim Biophys Acta* 1799:119–130.
41. Wang H, et al. (1999) HMG-1 as a late mediator of endotoxin lethality in mice. *Science* 285:248–251.
42. Campana L, Bosurgi L, Bianchi ME, Manfredi AA, Rovere-Querini P (2009) Requirement of HMGB1 for stromal cell-derived factor-1/CXCL12-dependent migration of macrophages and dendritic cells. *J Leukoc Biol* 86:609–615.
43. Yanai H, et al. (2009) HMGB proteins function as universal sentinels for nucleic-acid-mediated innate immune responses. *Nature* 462:99–103.
44. Kazama H, et al. (2008) Induction of immunological tolerance by apoptotic cells requires caspase-dependent oxidation of high-mobility group box-1 protein. *Immunity* 29:21–32.

Rheumatol Int (2011) 31:967–969
DOI 10.1007/s00296-010-1634-8

SHORT COMMUNICATION

S1P-targeted therapy for elderly rheumatoid arthritis patients with osteoporosis

Junichi Kikuta · Kaori Iwai · Yukihiko Saeki · Masaru Ishii

Received: 26 April 2010 / Accepted: 14 November 2010 / Published online: 28 November 2010

Abstract Therapeutics targeting sphingosine-1-phosphate (S1P), a kind of lipid mediator regulating immune cell trafficking, has been emerging rapidly as a novel line of regimen for autoimmune diseases, including rheumatoid arthritis (RA). Here, we propose that S1P-targeted therapy is beneficial not only for limiting inflammation but for preventing bone-resorptive disorders, such as osteoporosis, by controlling the migratory behavior of osteoclast precursors and therefore would be good for treating elderly female RA patients who suffer from postmenopausal osteoporosis and arthritis simultaneously.

Keywords Rheumatoid arthritis · Osteoporosis · Sphingosine-1-phosphate

The emergence of biological agents has undoubtedly caused a paradigm shift in the treatment of rheumatoid arthritis (RA). We rheumatologists are now ambitiously aiming at a 'cure', and not just the 'care', of RA patients and have succeeded in many cases [1]. Despite the brilliant victory over this intractable disease, there are still a large number of underprivileged patients who cannot share in these advances. Elderly RA patients are the main group; many of them cannot receive biological agents due to the high frequency of occurrence of life-threatening infections. Instead, they are treated with less efficacious disease-modifying antirheumatic drugs (DMARDs) and corticosteroids. Oral corticosteroids are still commonly used in clinical practice to relieve inflammation, but this can lead to systemic dysfunction because of the progressive joint damage, which is complicated by severe osteoporosis that increases the vulnerability to fractures of the spine and femur. Recent findings provide such patients with a ray of hope.

Sphingosine-1-phosphate (S1P), a lipid mediator enriched in blood, is a critical regulator of the migration and localization of various cell types, including immune cells [2]. Extensive studies have demonstrated that lymphocytes express $S1P_1$/Edg-1, a cognate receptor for S1P, which is responsible for their recirculation from lymphoid tissues to the systemic circulation [3]. S1P attracted lot of attention from rheumatologists when FTY720 (Fingolimod), a substance isolated from a Chinese herb and long known to have immunomodulating activity, was shown to be an S1P receptor agonist [4]. Although the detailed mechanism remains elusive, FTY720 acts as an S1P receptor agonist when metabolized and is now emerging as a promising novel immunosuppressive drug that presumably acts by limiting effector lymphocyte egress from lymph nodes. FTY720 is currently being tested clinically in autoimmune diseases such as multiple sclerosis [5], and many other S1P-targeted drugs (S1P receptor agonists or S1P lyase inhibitor) are beginning to be evaluated [6].

Recently, we have demonstrated that S1P was also important for controlling the migration of osteoclasts and their precursors [7]. Using an elaborate intravital two-photon microscopy imaging technique, the migratory behavior of osteoclast precursors in live bone tissues was shown to be critically regulated by S1P, and the intravenous application of an S1P receptor agonist rapidly promoted their exit from bone into blood [8]. It was also

J. Kikuta · K. Iwai · Y. Saeki · M. Ishii
Department of Rheumatology and Clinical Research, National Osaka-Minami Medical Center, Osaka, Japan

J. Kikuta · M. Ishii (✉)
Laboratory of Biological Imaging, WPI-Immunology Frontier Research Center, Osaka University, 3-1 Yamada-oka, Osaka, Suita 565-0871, Japan
e-mail: mishii@ifrec.osaka-u.ac.jp

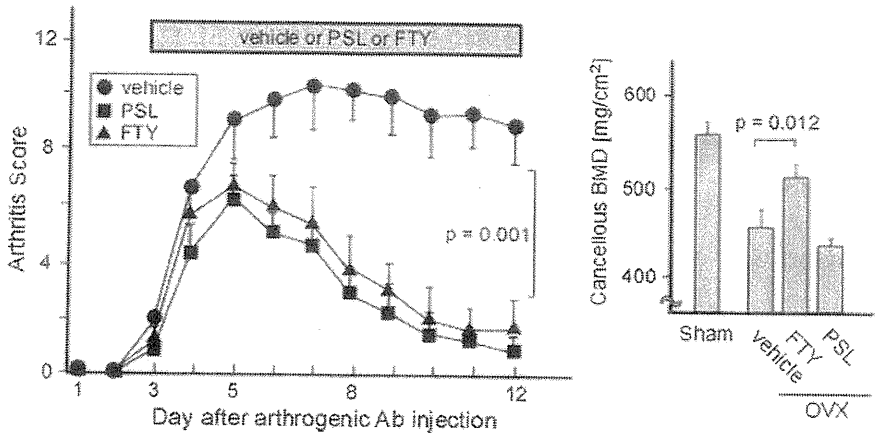

Fig. 1 The therapeutic effects of prednisolone (PSL) and FTY720 (FTY) in mice with both arthritis and osteoporosis. First, 8-week-old ovariectomized mice were injected with 5 mg of an arthrogenic anti-collagen II antibodies cocktail (Chondrex, Redmond, WA) at day 0, and then with 50 μg of lipopolysaccharide (LPS) (0111:B4, Sigma–Aldrich, St. Louis, MO) 3 days later (9). Prednisolone (PSL, 0.5 mg/kg/day), FTY720 (1 mg/kg/day), or vehicle only was administered every day beginning on day 3. The arthritis scores are shown in the left panel. The *error bars* represent the SEM ($n = 5$ per group). The cancellous bone mineral density (BMD) of the femur was analyzed by pQCT (LCT-200, Aloka, Japan) after killing the mice at day 14. *Error bars* represent the SEM ($n = 5$ per group)

demonstrated that treatment with the S1P receptor agonist FTY720 relieved ovariectomy-induced osteoporosis in mice (a model of postmenopausal osteoporosis in women), by facilitating osteoclast recirculation into blood and reducing the number of mature osteoclasts attached to the bone surface, which suggests a new line of therapy against bone-resorptive disorders [7]. These studies suggest that S1P-targeted therapy would be particularly beneficial for treating RA patients with both immunological and bone-resorptive disorders.

Inspired by this concept, we further examined the therapeutic effect of the S1P receptor agonist FTY720 on simultaneous disease involving both arthritis and osteoporosis (Fig. 1). Ovariectomized mice were injected with an arthrogenic anti-collagen II antibodies cocktail and then with lipopolysaccharide (LPS), so that they developed arthritis in their paws [9]. These mice exhibit both arthritis and osteoporosis and can be regarded as a model of elderly female RA patients. To treat the arthritis, prednisolone (PSL, 0.5 mg/kg/day), FTY720 (1 mg/kg/day), or vehicle only, was administered every day beginning on day 3, and the arthritis score was calculated [10]. We also evaluated bone mineral homeostasis by analyzing the cancellous bone mineral density (BMD) of the femur on day 14. The results showed that the S1P receptor agonist FTY720 was as potent as corticosteroid for suppressing arthritis; in addition, FTY720 recovered the ovariectomy-induced bone density loss, whereas prednisolone did not. As expected, these results clearly suggest that S1P-targeted therapy, such as with S1P receptor agonists, would be beneficial for treating elderly female RA patients who suffer from postmenopausal osteoporosis and arthritis simultaneously.

The effect of S1P receptor agonists is very rapid [4], and robust immunosuppressive effects (by sequestering lymphocytes) can be observed within a few hours after oral administration, although they do not last long (usually disappearing within 12–24 h). Therefore, the profile of an S1P receptor agonist would be similar to that of corticosteroid, rather than to those of methotrexate or other DMARDs. A variety of anticipated S1P-targeted drugs might replace corticosteroids for relieving the inflammation of RA and become a part of the standard RA treatment in the near future. This would be especially conducive to improving the quality of life of elderly patients, who have been left behind so far.

References

1. Van Volenhoven RF (2009) Treatment of rheumatoid arthritis: state of the art 2009. Nat Rev Rheumatol 5:531–541
2. Rosen H, Sphingosine Goetzl EJ (2005) 1-phosphate and its receptors: an autocrine and paracrine network. Nat Rev Immunol 5:560–570
3. Matloubian M, Lo CG, Cinamon G, Lesneski MJ, Xu Y, Brinkmann V et al (2004) Lymphocyte egress from thymus and peripheral lymphoid organs is dependent on S1P receptor 1. Nature 427:355–360
4. Mandala S, Hajdu R, Bergstrom J, Quackenbush E, Xie J, Milligan J et al (2002) Alteration of lymphocyte trafficking by sphingosine-1-phosphate receptor agonists. Science 296:346–349
5. Kappos L, Antel J, Comi G, Montalban X, O'Connor P, Polman CH et al (2006) on behalf of the FTY720 D2201 Study Group. Oral fingolimod (FTY720) for relapsing multiple sclerosis. N Engl J Med 355:1124–1140
6. Japtok L, Kleuser B (2009) The role of sphingosine-1-phosphate receptor modulators in the prevention of transplant rejection, autoimmune diseases. Curr Opin Investig Drugs 10:1183–1194

7. Ishii M, Egen JG, Klauschen F, Meier-Schellersheim M, Saeki Y, Vacher J et al (2009) Sphingosine-1-phosphate mobilizes osteoclast precursors and regulates bone homeostasis. Nature 458:524–528
8. Klauschen F, Ishii M, Qi H, Bajénoff M, Egen JG, Germain RN et al (2009) Quantifying cellular interaction dynamics in 3D fluorescence microscopy data. Nat Protoc 4:1305–1311
9. Terato K, Hasty KA, Reife RA, Cremer MA, Kang AH, Stuart JM (1992) Induction of arthritis with monoclonal antibodies to collagen. J Immunol 148:2103–2108
10. Sasai M, Saeki Y, Ohshima S, Nishioka K, Mima T, Tanaka T et al (1999) Delayed onset and reduced severity of collagen-induced arthritis in interleukin-6-deficient mice. Arthritis Rheum 42:1635–1643

JACS
JOURNAL OF THE AMERICAN CHEMICAL SOCIETY

ARTICLE

pubs.acs.org/JACS

In Vivo Fluorescence Imaging of Bone-Resorbing Osteoclasts

Toshiyuki Kowada,[†] Junichi Kikuta,[‡,§] Atsuko Kubo,[‡,§] Masaru Ishii,[‡,§] Hiroki Maeda,[¶] Shin Mizukami,[†,¶] and Kazuya Kikuchi*[,†,¶]

[†]Laboratory of Chemical Imaging Techniques, Immunology Frontier Research Center (IFReC), Osaka University, Osaka, Japan
[‡]Laboratory of Cellular Dynamics, Immunology Frontier Research Center (IFReC), Osaka University, Osaka, Japan
[§]Japan Science and Technology Agency (JST), CREST, Tokyo, Japan
[¶]Department of Material and Life Science, Graduate School of Engineering, Osaka University, Osaka, Japan

Supporting Information

ABSTRACT: Osteoclasts are giant polykaryons responsible for bone resorption. Because an enhancement or loss of osteoclast function leads to bone diseases such as osteoporosis and osteopetrosis, real-time imaging of osteoclast activity in vivo can be of great help for the evaluation of drugs. Herein, pH-activatable chemical probes BAp-M and BAp-E have been developed for the detection of bone-resorbing osteoclasts in vivo. Their acid dissociation constants (pK_a) were determined as 4.5 and 6.2 by fluorometry in various pH solutions. These pK_a values should be appropriate to perform selective imaging of bone-resorbing osteoclasts, because synthesized probes cannot fluoresce intrinsically at physiological pH and the pH in the resorption pit is lowered to about 4.5. Furthermore, BAp-M and BAp-E have a bisphosphonate moiety that enabled the probes to localize on bone tissues. The hydroxyapatite (HA) binding assay in vitro was, therefore, performed to confirm the tight binding of the probes to the bone tissues. Our probes showed intense fluorescence at low pH values but no fluorescence signal under physiological pH conditions on HA. Finally, we applied the probes to in vivo imaging of osteoclasts by using intravital two-photon microscopy. As expected, the fluorescence signals of the probes were locally observed between the osteoclasts and bone tissues, that is, in resorption pits. These results indicate that our pH-activatable probes will prove to be a powerful tool for the selective detection of bone-resorbing osteoclasts in vivo, because this is the first instance where in vivo imaging has been conducted in a low-pH region created by bone-resorbing osteoclasts.

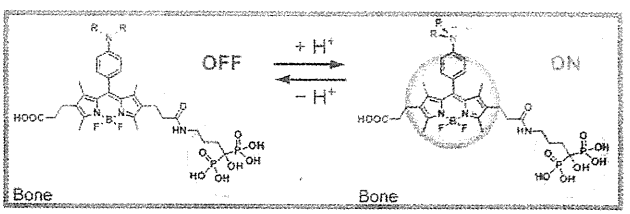

INTRODUCTION

Osteoclasts are giant multinucleated cells derived from monocytoid hematopoietic cells, which are responsible for bone resorption within the bone-remodeling compartment.[1−4] Because an enhancement or loss of osteoclast function causes bone diseases such as osteoporosis or osteopetrosis, real-time imaging of osteoclast activity in vivo is one of the most important tools required for investigations of osteoclast functions.[4] However, current bone imaging techniques such as computed tomography (CT) and biochemical markers of bone metabolism cannot connect spatial information with cellular activity. To overcome this problem, fluorescence imaging is a promising technique for obtaining temporal and spatial information about target cells or proteins.[5] Thus, we sought to develop fluorescent chemical probes with an OFF/ON switch, which can selectively detect active osteoclasts and thereby instantaneously provide an image of the location of the osteoclasts activated by particular stimuli. Furthermore, two-photon excitation microscopy can provide noninvasive imaging of osteoclasts in vivo.[6]

Active osteoclasts resorb the organic and inorganic components of the bone tissues by cathepsin K secretion and by proton extrusion, which causes acidification of the bone surface.[4] To the best of our knowledge, there have been no reports on the detection of protons extruded by osteoclasts. Only a single report has demonstrated the indirect in vivo detection of cathepsin K activity.[7] However, the cathepsin K probe has not yet provided real-time imaging data about the osteoclasts in the process of resorbing bone tissues, and its selectivity as a probe for the detection of osteoclast formation is inadequate.

We recognized that active osteoclasts can be selectively detected through specific imaging of low-pH regions by using a pH-activatable fluorescent probe[8] with specific delivery of the probe using a bisphosphonate group[9] (Figure 1a). In addition, this probe should be quite useful in the evaluation of drugs.

There are two requirements for the development of new probes for selective detection of bone-resorbing osteoclasts. One obvious requirement is a pH-sensitive fluorescence switch, and the other is the capability to localize on the bone tissue. Therefore, we designed fluorescent probes called "BAps". These probes are composed of boron−dipyrromethene (BODIPY) dye and a bisphosphonate group (Figure 1b). BODIPY dyes are

Received: July 12, 2011
Published: September 22, 2011

   dx.doi.org/10.1021/ja2064582 | J. Am. Chem. Soc. 2011, 133, 17772–17776

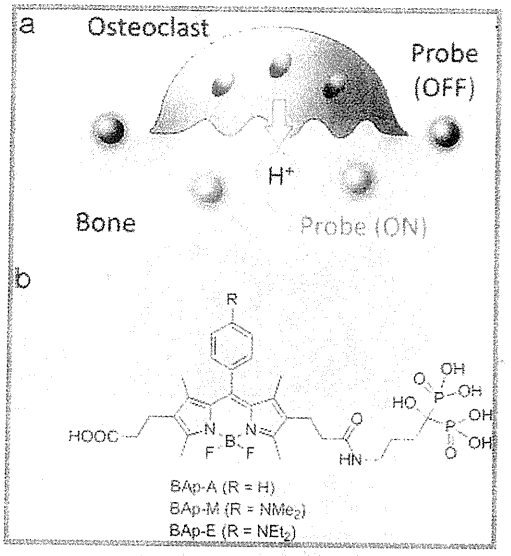

Figure 1. Strategy for selective detection of bone-resorbing osteoclasts using pH-activatable probes and design of BAps. (a) pH-activatable probes are immobilized on the bone tissue and provide intense fluorescence only when osteoclasts are resorbing bone. (b) Structures of the pH-activatable probes (BAps).

well-known fluorophores that have been used in a large number of applications because of their environmental stability, large molar absorption coefficients, and high fluorescence quantum yields.[10] Most recently, pH-activatable fluorescence probes including a BODIPY dye have been developed for the detection of cancers and real-time monitoring of therapy.[11] Furthermore, bisphosphonate compounds are currently used as drugs for the treatment of various bone diseases. These compounds chelate calcium and inhibit bone resorption. We, therefore, decided to combine a BODIPY-based pH-sensing unit with a bisphosphonate compound.

RESULTS AND DISCUSSION

Characterization of BAps. To demineralize the bone matrix, osteoclasts secrete protons (H^+) into the resorption pit where the pH value is lowered to about 4.5.[3] We, therefore, considered that selective imaging of osteoclasts would be achieved by the development of pH-activatable probes with an acid dissociation constant (pK_a) in the range of 4.5−6.5, because those probes cannot intrinsically fluoresce at the physiological pH. According to this assumption, we designed and synthesized three fluorescent probes with different pK_a values (Figure 1b). A control probe with "always-ON" fluorescence (BAp-A) was developed. The other probes are fluorescence "turn-ON" type sensors that can detect the acidic pH environment. Since the fluorescence OFF/ON switching mechanism is based on photoinduced electron transfer (PeT), the pK_a values of these probes can be finely tuned by the appropriate choice of an electron-donating moiety attached to the BODIPY core.[12] Thus, we chose *p*-dimethylanilino (BAp-M) and *p*-diethylanilino groups (BAp-E) as the electron-donating moieties to provide pK_a values in the range of 4.5−6.5.

The fluorescent probes were synthesized in one step from the corresponding dicarboxylic acids by using straightforward synthetic pathways (Scheme S1, Supporting Information). To confirm the pH-dependent fluorescence properties of BAps, we

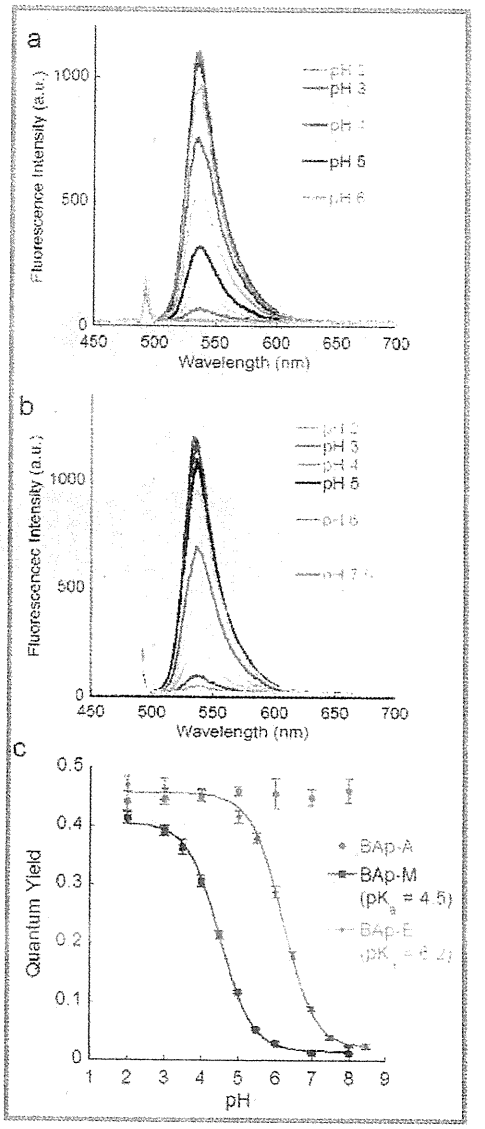

Figure 2. Fluorescence spectra (0.2 μM, excited at 492 nm) of (a) BAp-M and (b) BAp-E in citrate-phosphate buffer, and (c) pH-dependent profiles of changes in fluorescence quantum yield of BAps. The data were fitted to the Henderson−Hasselbalch equation.

measured the absorption and emission spectra in citrate-phosphate buffer at different pH values (Figures S1 and 2). All three probes had absorption maxima at about 520 nm. These peaks were found to be independent of the pH of the buffer. These results indicate that any structural changes or aggregations of the dye induced by pH changes do not occur in aqueous solution. In contrast, the fluorescence intensities of BAp-M and BAp-E were highly affected by the pH (Figure 2). The fluorescence intensities of BAp-M and BAp-E decreased along with an increase in pH. Essentially, no fluorescence was observed at the physiological pH. This phenomenon can be rationalized by the observation that PeT actually occurs from the *p*-anilino group to the BODIPY core.[12] Thus, these two probes showed a fluorescence "turn-ON" type increase at lower pH. Furthermore, the pK_a values were estimated by fitting pH-dependent changes of the fluorescence quantum yield to the

dx.doi.org/10.1021/ja2064582 |J. Am. Chem. Soc. 2011, 133, 17772–17776